

1 **Active tectonics of the Ganzi-Yushu fault in the southeastern Tibetan Plateau**

2 Feng Shi¹, Honglin He¹, Alexander L. Densmore², An Li³, Xiaoping Yang¹, Xiwei Xu¹

3 1 Key Laboratory of Active Tectonics and Volcano, Institute of Geology, China Earthquake

4 Administration, Beijing 100029, China.

5 2 Institute of Hazard and Risk Research and Department of Geography, Durham University,

6 Durham, UK.

7 3 Key Laboratory of Crustal Dynamics, Institute of Crustal Dynamics, China Earthquake

8 Administration, Beijing 100085, China.

9

10 **Abstract:** The ongoing convergence between India and Eurasia apparently is accommodated
11 not merely by crustal shortening in Tibet, instead also by motions along strike slip faults which are
12 usually boundaries between tectonic blocks, especially in the Tibetan plateau. Quantification of
13 this strike slip faulting is fundamental for understanding the collision between India and Eurasia.
14 Here, we use a variety of geomorphic observations to place constraints on the late Quaternary
15 kinematics and slip rates of the Ganzi-Yushu fault, one of the significant strike-slip faults in
16 eastern Tibet. The Ganzi-Yushu fault is an active, dominantly left-lateral strike-slip structure that
17 can be traced continuously for up to 500 km along the northern boundary of the clockwise-rotating
18 southeastern block of the Tibetan Plateau. We analyse geomorphic evidence for deformation, and
19 calculate the late Quaternary slip rates at four sites along the eastern portion of the fault trace.
20 Latest Quaternary apparent throw rates are variable along strike but are typically ~1 mm/a. Rates
21 of strike-slip displacement are likely to be an order of magnitude higher, 8-11 mm/a. Trenching at
22 two locations suggest that the active fault behaviour is dominated by strike-slip faulting and reveal

23 several earthquake events with refined information of timing. . The 2010 M_w 6.9 Yushu earthquake,
24 which occurred on the northwestern segment of the Ganzi-Yushu fault zone, provides additional
25 evidence for fault activity. These observations agree with GPS-derived estimates, and show that
26 late Quaternary slip rates on the Ganzi-Yushu fault are comparable to those on other major active
27 strike-slip faults in the eastern Tibetan Plateau.

28

29 **Keywords:** Ganzi-Yushu fault, late Quaternary, active faulting, slip rates, India-Asia collision

30

31 **1. Introduction**

32 The ongoing convergence between India and Eurasia apparently is accommodated not merely by
33 crustal shortening in Tibet, instead also by motions along strike slip faults which are usually
34 boundaries between tectonic blocks, especially in the Tibetan plateau [Molnar and Tapponnier,
35 1978]. To explain this deformation, two influential end-member views of continental deformation
36 have been debated during the last several decades: (1) block models, in which intracontinental
37 deformation can be concentrated on major faults separating a number of relatively rigid
38 blocks[e.g., Dewey et al., 1973; Avouac and Tapponnier, 1993; Peltzer and Saucier, 1996;
39 Tapponnier et al., 2001; Meade, 2007; Thatcher, 2007]; or (2) continuum models, in which
40 deformation is regionally distributed in the shallow brittle crust, and is essentially continuous at
41 depth[e.g., Molnar and Tapponnier,1975; England and McKenzie, 1982; England and Houseman,
42 1986;]. When the two views are applied to eastern Asia, large slip rates on major faults are
43 required by block models, but not by continuum models. Thus, documentation and quantification

44 of kinematics and slip rates on the major strike slip faults, along with observations of historical
45 earthquake activity, are fundamental for understanding the collision between India and Eurasia.

46

47 The four major earthquakes ($M_w > 7.0$) which occurred in the Tibetan Plateau during the last two
48 decades (1997 $M_w 7.5$ Manni earthquake [Xu, 2000], 2001 $M_w 7.8$ Kunlunshan earthquake [Xu et
49 al., 2002], 2008 $M_w 7.2$ Yutian earthquake [Xu et al., 2011] and 2008 $M_w 7.9$ Wenchuan earthquake
50 [Xu et al., 2009]), and the 2010 $M_w 6.9$ Yushu earthquake, all occurred around the boundaries of
51 the Bayan Har fault-block (Figure 1), also known as the Songpan block [Thatcher, 2007] or
52 Kunlun block [Gan et al., 2007], surrounding by Longmenshan Fault (east boundary),
53 Xianshuihe Fault and Ganzi-Yushu fault (south boundary), Kunlun fault (north boundary). The
54 published GPS velocities [e.g. Wang et al., 2001; Gan et al., 2007; Thatcher, 2007] suggest the
55 southward movement of the Bayan Har fault-block relative to stable Eurasia, but the mechanisms
56 and starting time of this movement have been a matter of debate [Chen et al., 1994; Kirby et al.,
57 2000, 2002, 2003; Clark et al., 2005]. The eastern boundary faults of the block accommodated
58 significant crustal shortening during the Late Triassic Indosinian Orogeny [Chen and Wilson, 1996;
59 Li et al., 2003], and the Longmen Shan region at the eastern margin of the block has been
60 identified as a major thrust zone that was reactivated in the India-Asia collision [e.g., Avouac and
61 Tapponnier, 1993; Xu and Kamp, 2000]. The northern and southern boundaries of the block are
62 major left-lateral strike-slip faults – the Ganzi-Yushu and Xianshuihe fault system to the south,
63 and the Kunlun fault system to the north.

64

65 In order to understand the mechanism of the Bayan Har fault-block in the India-Asia collision, the

66 late Cenozoic activity and kinematics of the major faults along the block margins must be
67 documented. Much work about the late Cenozoic activity and kinematics of faults in the Longmen
68 Shan has been done by Chen et al. [1994], Burchfiel et al. [1995] and Densmore et al. [2007]. The
69 slip rates of the Xianshuihe and Kunlun faults have been well constrained [e.g. Allen et al., 1991;
70 Van der Woerd et al., 2002], there are also many results of slip rate on Ganzi-Yushu fault from
71 fieldwork [Zhou et al., 1996; Wen et al. 2003; Peng et al., 2006] and GPS [Wang et al., 2001; Shen
72 et al., 2005; Gan et al., 2007; Wang, 2009]. Tapponnier et al. [2001] and others inferred fast rates,
73 about 15 mm/a, to argue for rigid-block extrusion, but others [e.g., England and Molnar, 2005]
74 have suggested that slow rates, about 5 mm/a or slower, are consistent with continuous
75 deformation. The kinematics of the Ganzi-Yushu fault, its slip rate, and the timing of
76 paleoearthquakes on the fault all remain poorly constrained. Some slip rates have been obtained
77 from terrace or alluvial fan offsets along with age estimates from TL (thermoluminescence) dating
78 [Zhou et al., 1996; Wen et al. 2003]. There has also been some work using river offsets, although
79 the ages of these offsets were only loosely constrained as Holocene [Peng et al., 2006]. The huge
80 range of the slip rates, which from 3 mm/a to 13 mm/a, couldn't test different deformation models.
81 The reasons of the huge range come from two aspect, one is the dating method and another is the
82 choice of offset markers. Moreover, because of the high altitude and remoteness of the fault,
83 there has been very little work on paleoearthquakes in these areas.

84

85 We address the fault trace by presenting geomorphic evidence for deformation along the
86 Ganzi-Yushu fault, and constrain the fault behaviour by paleoseismology. We use a combination of
87 techniques, including field mapping, image interpretation, surveying of offset geomorphic markers,

88 and trenching, in order to examine the history of fault slip over the last few thousand years.

89 **2 Geological setting**

90 The Ganzi-Yushu fault zone forms part of the boundary between the Qiangtang and Bayan Har
91 blocks in the eastern Tibetan Plateau [Zhang et al., 2003; He et al., 2006]. The Ganzi-Yushu fault
92 zone can be traced for ~500 km along strike and consists of a series of generally NW-striking fault
93 segments. The western most tip of the fault zone occurs near Qutang township, in Zhiduo county
94 of Qinghai Province, and the fault extends eastward through Dangjiang, Yushu, Dengke, and
95 Yulong townships to end at Ganzi county in Sichuan Province. Where it is visible at the surface,
96 the fault appears to dip 70-85°NE near the surface, except for a SW-dipping segment near
97 Tuodang township [Li et al., 1995]. The 2010 M_w 6.9 Yushu earthquake ruptured the Ganzi-Yushu
98 fault over a total distance of about 50 km [Chen et al. 2010; Li et al., 2012]. Focal mechanism
99 solutions [Chen, 2010; USGS, 2010] and displaced geomorphic features indicate that the
100 earthquake rupture is nearly pure left-lateral strike-slip with a minor SW dip-slip component.

101 Exposures of the active Ganzi-Yushu fault show that it coincides with zones of dense fracturing in
102 pre-Quaternary bedrock; the widths of these zones is generally ~10-50 m but is rarely up to a few
103 hundred meters [Zhou et al., 1996]. In remote sensing imagery, strands of the fault form clear
104 linear features associated with scarps, shutter ridges, and offset drainages characteristic of active
105 strike-slip deformation [Zhou et al., 1996]. The fault movement appears to be dominated by
106 left-lateral strike-slip, with little consistent net vertical slip [Peng et al., 2006].

107 Previously-published estimates of strike-slip rates span a large range from 3 mm/a to 14 mm/a
108 (Figure 2) [Zhou et al., 1996; Wen et al., 2003; Peng et al., 2006]. Many of these are based on

109 low-resolution geomorphic markers (e.g., river offsets) and on imprecise or relative dating
110 techniques. Based on GPS velocities, the Ganzi-Yushu fault has an estimated strike-slip rate of 10
111 mm/a to 16 mm/a, depending on the tectonic model that is used (Figure 2) [Wang et al., 2001;
112 Shen et al., 2005; Gan et al., 2007; Wang, 2009].

113

114 **3 Methods and techniques**

115 **3.1 Fault mapping**

116 We focus our attention on the southeastern 150 km of the Ganzi-Yushu fault zone. This is because
117 (1) the northwestern strands of the fault are relatively inaccessible, and (2) Quaternary deposits
118 that could be used to indicate the kinematics and timing of recent deformation are more
119 extensively exposed along the southeastern portion of the fault zone (Figure 1). We mapped the
120 active traces of the southeastern Ganzi-Yushu fault zone with CBERS (China-Brazil Earth
121 Resources Satellite) imagery (2.36 m spatial resolution) and Chinese aerial photographs (~1 m
122 spatial resolution). We then made field observations at sites with geomorphic indicators of late
123 Quaternary activity, including scarps or offset surfaces in Quaternary deposits, offset channels,
124 shutter ridges and linear valleys. Offset landforms were surveyed using a differential GPS (DGPS)
125 measuring system, with a measurement repeatability of better than ± 10 cm. If the offsets were too
126 large to be measured by field surveys, we estimated the offsets from the CBERS imagery and
127 aerial photographs.

128

129 Much of the evidence for active faulting comes from offset or truncated fluvial fill terraces. We
130 mapped these terraces on aerial photographs, supplemented with field investigations. Fill terraces
131 in this region are typically composed of subhorizontal, crudely- to well-bedded gravel and sand
132 layers. We identified terrace surfaces, and assigned relative ages, on the basis of relative height
133 between the surface and the modern river bed. At each site, terraces were numbered in ascending
134 order from youngest (T0, representing the modern floodplain) to oldest. We determined absolute
135 ages of fill terrace deposition and abandonment using ^{14}C dating of samples in sand layers. We
136 lack sufficient data to assess whether terrace ages can be correlated between different sites along
137 the Ganzi-Yushu fault, or whether the terrace chronology is site-specific.

138

139 Although the strike-slip component is dominant along the entire fault, the ratios of strike-slip
140 and vertical offsets, and the strike-slip rates, are not uniform along strike. With this in mind, we
141 describe our observations below in terms of strike-slip and vertical offsets. Throw rates are
142 regarded as consistent along each fault segment, but the ratio and the strike-slip rates have a
143 tendency to decline from west to east, toward the fault tip.

144

145 **3.2 Trenching**

146 To establish the timing of the most recent slip on the fault, we excavated several trenches across
147 the Ganzi-Yushu fault at two separate sites. Accurate fault traces and sufficient sediment
148 accumulation with organic material are fundamental for trenching. In Renguo township (Figure 2),
149 we excavated a 2-m-deep trench across the fault. This site is located at a well-developed fault

150 scarp on a terrace surface near the estimated epicenter of the 1854 earthquake [Wen et al., 2003].
151 The steep terrain south of the site has trapped sediment, providing sufficient organic material.
152 Because a distinctive layer was found in the west wall of the trench, but not in the east wall, we
153 excavated a second 2-m-deep trench at right angles to the first, parallel to the fault, in order to
154 reconstruct a horizontal piercing line. To assess possible differences in fault activity between
155 different segments, we excavated a 3-m-deep trench across the fault at Cuoia township (Figure
156 2). This site is also located on a terrace surface. The fault plane is exposed in the terrace riser,
157 allowing accurate determination of the fault position, and the steep terrain to the south of the site
158 provides sufficient sediment accumulation and organic material. All trench walls were cleaned and
159 logged at a scale of 1:10 following standard procedures [e.g., McCalpin, 1996]. Depositional ages
160 of the units in the trench faces were provided by ^{14}C analysis of charcoal fragments from Beta
161 Analytic Radiocarbon Dating Laboratory.

162 **4 Results**

163 We can trace the southeastern Ganzi-Yushu fault continuously for approximately 150 km. The
164 fault shows clear evidence for Quaternary sinistral strike-slip displacement, with minor
165 components of dip slip.

166 **4.1 Shengkang**

167 Shengkang (Figure 2) was severely damaged by the 1854 earthquake [Wen et al., 2003]. On aerial
168 photographs, there are obvious offsets of fill terraces at this site (Figure 3). The fault has caused
169 sinistral strike-slip displacement of the T5/T3 riser by approximately 350 m, and a vertical offset

170 of the T5 surface by ~50 m (Figure 3).The ages of T5 and T3 at this site have been estimated at
171 46100 ± 3500 a and 16290 ± 1200 a based on TL dating [Wen et al., 2003]. But Wen et al. [2003]
172 estimate the sinistral-slip rate as 11.5 ± 2.4 mm/a using the mean date between ages of T5 and T3,
173 and inistral strike-slip displacement of the T5/T3 riser, and not estimate the throw rate. The age of
174 T5 is older twice than the age of T3, and the difference between the ages of T5 and T3 is nearly
175 30000 a. Base on geomorphologic analysis, we hold the opinion that estimating the sinistral-slip
176 rate of 8 ± 1 mm/a and the throw rate of 1 ± 0.1 mm/a using the age of T5 is more suitable. No
177 other clear terrace offsets are preserved at this site.

178

179 **4.2 Renguo**

180 Near Renguo township, a fault scarp let probably associated with the 1854 earthquake, trending
181 300° with a height of 0.5-1.5m, can be traced for 3 km across on a gently sloping piedmont (Figure
182 4a, b, c). The fault scarp extends southeast to Ezhong village and dislocates a footpath (Figure 4f),
183 which was built in an ephemeral gully. The eastern boundary of the path shows a sinistral offset of
184 3m, as does the gully axis. The fault scarp extends northwest to Kagong township and produces a
185 200m long sag-pond (Figure 4d). According to the leader of Renguo village, there was a village in
186 this region in the past, which was abandoned about 100 years ago. This event may be related to the
187 occurrence of the earthquake in 1854, with an epicenter located near Renguo township [Wen et al.,
188 2003].

189

190

191 The trench at Renguo township was excavated across the fault scarp (Figure 3). Six distinct
192 lithologic units were identified in the trench walls, and are described in detail in Table 1. Four
193 fault planes have been recognized in the trench: Fault F1 cuts the lower units and terminates in
194 U1-1. No wedge or flower structure are found at the upper termination of the fault plane. Faults F2
195 cuts unit U1-1, and is overlain by scarp-fill wedges A and B. Scarp-fill edge A is dislocated by F2
196 in the east wall of RGTC1, while some gravel is aligned along the fault in the west wall of RGTC1
197 (Figure 4a). Fault F3 cuts unit U1-1, and appears to terminate at the base of U2. The fault is
198 expressed as a disturbed zone 10-15 cm wide, and creates an uneven base of U2. Fault F4 cuts
199 units U1-1, U2, and U3, and appears to terminate at the base of U4-1. On the east wall of the
200 trench, the fault is associated with an irregularly-shaped deposit of massive or structure less fine
201 gravel.

202

203 Examination of both the fault-normal and fault-parallel trench walls shows that unit U3 pinches
204 out to the east on both the northeast and southwest sides of the fault (Figure 5e). We use the
205 pinch-out position as a piercing line, and estimate that it has been offset by 7.5 ± 0.5 m of sinistral
206 strike-slip and 1 ± 0.2 m of vertical displacement, with the southern or hanging wall block
207 upthrown.

208

209 We infer that two paleoearthquake events are recorded in the Renguo trenches. The first
210 paleoearthquake event occurred after U1 was deposited. Faults F2 and F3 were activated and
211 wedge A was deposited over F2 in this event. The overlying layer U2 is disturbed and has an
212 undulating base over fault F3. We interpret that U2 was being actively deposited when the first

213 paleoearthquake event occurred and continued to deposit after the earthquake. For this reason, U2
214 is only deformed near its base, and becomes more flat-lying further up-section. A ^{14}C sample from
215 the base of U2 yields an age of 3030-2885 BC. This is a maximum age for the first
216 paleoearthquake event. The second event occurred after U3 had been deposited, and is marked by
217 dislocation of unit U3 by F4 on the west wall of the trench. This may have been accompanied by
218 remobilization of U3 gravel as a massive deposit along F4. F4 is not clear on the east wall, and no
219 evident deformation was seen in unit U3, which does not appear in the footwall. The gravel deposit
220 along F4 yields a ^{14}C age of 905-795 BC, while a sample from U3 yields an age of 770-475 BC.
221 We use OxCal 4.2.4 (Bronk Ramsey, 2013) by 6 ^{14}C age (RGTC1-W6, RGTC1-E1, RGTC1-W9,
222 RGTC1-W16, RGTC1-E17, RGTC1-E16) to estimate the two events: event E1 (7230-3015 BC)
223 and event E2 (885-525 BC) (Figure. 6). The sinistral-oblique offset of the U3 pinch-out must be
224 due to displacements in two seismic events: the second paleoearthquake event mentioned above,
225 and the historical earthquake in 1854 that produced a 3 m displacement on the Ezhong footpath.
226 Using the measured sinistral-oblique offset of the U3 pinch-out and the ages of samples within
227 and overlying U3 (770-475 BC and 985-1155 AD), the sinistral-slip rate is estimated to be
228 between 2.9 ± 0.3 mm/a and 8.0 ± 0.3 mm/a, and the throw rate is between 0.4 ± 0.1 mm/a and 1.1
229 ± 0.1 mm/a.

230

231 **4.3 Cuo**

232 There are three terraces at Cuo village, all cut by the Ganzi-Yushu fault. T3 and T2 are only
233 preserved on the west side of the river. The vertical dislocation between hanging wall and footwall

234 is 8m on the T3 terrace and 2-3 m on the T2 terrace, and the T3/T2 riser is offset in a sinistral
235 sense by about 80 m. The fault is exposed on the west side of the river, where it places Triassic
236 slate and metasandstone of the southwest (hanging wall) block over Quaternary sand and gravel of
237 the northeast (foot wall) block. The fault dips 68° toward 305° (Figure 7d).

238 The CATC1 trench was excavated in the T2 terrace near Cuoia township (Figure 7b), perpendicular
239 to a 2 m fault scarp. The hanging wall is composed primarily of bedrock on the southwestern side
240 of the fault, overlain by units U4 and U5 (Figure 8). The presence of resistant bedrock at the
241 hanging wall has allowed accumulation of at least two distinct sediment wedges in the footwall,
242 along with unit U3. The fault is expressed in both walls of the trench as a positive flower structure
243 with a general dip to the southwest, and five separate fault planes can be identified:

244

245 Fault F1 cuts unit U3 and appears to terminate at the base of U4 on the east wall of CATC1. On
246 the west wall, however, F1 terminates at the base of U3. Fault F2 cuts unit U3 and U4 on the east
247 wall, but only cuts unit U3 on the west wall. Fault F3 is only visible at the east wall of CATC1. It
248 cuts unit U4 and wedge A, and appears to terminate at the base of U5. The fault is divided into two
249 branches within wedge A, leading to about 10-20 cm vertical offset of the top surface of wedge A.

250 Fault F4 cuts unit U4, wedge A and wedge B, and appears to terminate at the base of U5. Fault F5
251 cuts unit U4, wedge A and wedge B on the east wall, but on the west wall, it is covered by wedge
252 B. We infer that two paleoearthquake events are recorded in the CATC1 trench, both of which
253 post-date deposition of units U1, U2 and U3. We use OxCal 4.2.4 (Bronk Ramsey, 2013) by 6^{14}C
254 age (CATC1-W6, CATC1-E5, CATC1-E3, CATC1-W3, CATC1-W4, CATC1-E4) to estimate the
255 two events: event E1 (3580-2640 BC) and event E2 (2135-1510 BC) (Figure 9). The first event

256 involved faults F1 and F2, and formed wedge A between U1 and U3. Materials in the wedge
257 appear to have been derived from U3 (Figure 10b). Samples from the upper portion of U3 and
258 from wedge A indicate that the lower limit time on the first paleoearthquake is 3655-3515 BC and
259 the upper limit time is 2780-2560 BC (Figure 8). Unit U4 was deposited after the first event. The
260 second paleoearthquake event occurred after deposition of unit U4, and involved faults F4 and F5
261 (Figure 10c). Expressions of the second event are different on the two walls of the CATC1 trench.
262 Slip on F3 appears to have resulted a suite dislocates in wedge A and slip on F2 appears to have
263 resulted in wedge A slipping down between F2 and F4 on the east wall. The overlying layer U4
264 collapsed, allowing deposition of wedge B between F4 and F5. In contrast, F3 shows no signs of
265 rupture in the second paleoearthquake on the west wall of the trench. Instead, F4 dislocated U4
266 and wedge B was formed above unit U4 in the hanging wall (Figure 10d). The upper and lower
267 limit times for the second paleoearthquake are constrained by ^{14}C ages on wedge B of 1620-1435
268 BC and on U4 of 2210-1975 BC (Figure 8). The surface layer U5 was deposited after the second
269 event, and yields a ^{14}C age of 1150-1275 AD (Figure 10e).

270

271 The epicenter of the M~8 Zhuqin-Ria earthquake in AD1320 is thought to be near to the CATC1
272 trench [Zhou et al., 1997]. The bulges and small scarps developed on the T2 surface at Cuo
273 (Figure 8d) may be related to this historical earthquake, which occurred after the deposition of U5.
274 However, we do not see direct evidence of this earthquake in the trench.

275

276 Because of abundant ^{14}C samples from CATC1 on T2 and obvious offsets of the T2 surface, T2 is
277 thus an extremely well-suited place to determine the fault slip rate. We use the sinistral offsets of

278 the T3/T2 riser and the T2 age to evaluate the sinistral-slip rate, and the throw rate is evaluated
279 from the height of scarp on T2 and the T2 age. The sinistral and vertical offsets, as obtained from
280 DGPS surveys, are 80 m and 2.5 m, respectively. If we use the age (6115-5970 BC) of sample
281 CATC1-E4 (see Figures 7 and 8 for location) in unit U3 of CATC1 to approximate the T2 age,
282 then the sinistral-slip rate and throw rate are 10 ± 0.4 mm/a and 0.3 ± 0.1 mm/a. Note that this is a
283 minimum age for the T2 fill terrace, because the riser formed before any of the T2 deposits were
284 load down, so this is maximum limiting slip rate.

285

286 **4.4 Ria**

287 Ria is located 30km to the northwest of Cuoia (Figure 2), and shows clear evidence of offset fill
288 terraces (Figure 11). We obtained horizontal and vertical offsets from field surveys. The T3/T2
289 riser is sinistrally offset by about 80 m, similar to the offsets of T3 terrace margins located about
290 500m to the southeast (Figure 11). The T2/T1 riser is sinistrally offset by about 20 m. The vertical
291 offsets of the T3 and T2 terrace treads are 10 m and 8 m, respectively. Wen et al. [2003] published
292 an estimate Holocene slip rates of 12 ± 8 mm/a in the horizontal and 1.2 ± 0.2 mm/a in the vertical
293 by T2 age.

294

295 **5 Discussion**

296 Our results provide clear evidence for late Quaternary oblique sinistral-thrust activity on the
297 southeastern Ganzi-Yushu fault at rates of 8 to 11 mm/a in the horizontal and 0.3 to 1.1 mm/a in

298 the vertical. These slip rates provide important constraints on the applicability of different tectonic
299 models for the present-day deformation of the Tibetan Plateau. Block models have been suggested
300 that actively deforming regions are comprised of blocks or microplates. Most deformation occurs
301 along major blocking faults, with minor faulting but little internal deformation of the blocks
302 themselves. So this model has been advocated primarily by geologists who cite evidence for high
303 (10-30 mm/a) slip rate on the major strike-slip faults of Tibet [e.g. [Avouac and Tapponnier, 1993](#)].
304 On the contrary, continuum models are viewed as quasi-continuous, governed by the fluid-like
305 solid-state flow of a viscous material. This model has been proposed primarily by geophysicists
306 using laboratory measurements to constrain the ductile flow properties of Earth's lithosphere, its
307 strong outer, ~100 km thick surface layer, and construct dynamical models of continental
308 deformation [e.g., [England and Molnar, 2005](#)]. In this view, discrete slip in the brittle upper crust
309 occurs on many faults with roughly comparable slip rates.

310

311 For many of the large strike-slip faults within the Indo-Asian collision zone [e.g. [Allen et al., 1991](#);
312 [Van et al., 2002](#)], slip rates determined geodetically are generally different to those reported using
313 reconstructions of offset landforms, and it is unclear if this discrepancy reflects true secular
314 variation in slip history, systematic errors in interpretation, or both. Even slip rates reported using
315 different reconstructions of offset landforms along the same fault are different. A major potential
316 source of uncertainty when assessing slip rates from offset fill terraces is the underlying
317 geomorphic model of terrace formation and abandonment that must be assumed [e.g., [Zhang et al.,](#)
318 [2004](#); [Cowgill, 2007](#)]. One evolutionary model suggests that the erosion of flood plain and its
319 banks continues until the river begins to incise and new terraces are formed [[Van et al., 2002](#)].

320 According to this model, offset of a terrace riser only begins to accumulate once the lower terrace
321 is abandoned. An alternative model allows for differences in erosion pattern between the sides of
322 the river, in which case riser offsets may begin to accumulate after the upper terrace is abandoned.

323

324 Based on our field observations, we suggest that, at different sites along the Ganzi-Yushu fault,
325 different models are most suitable. At Shengkang, the T5/T3 riser cannot be eroded because of its
326 location away from the position of the river (Figure 12a, b). So we use the offset of the T5/T3 riser,
327 divided by the abandonment age of T5, to calculate the slip rate. We cannot, however, use the
328 same method to calculate the slip rate at Ria, because the risers are subject to erosion by the river
329 (Figure 12c, d). Assuming that the offsets could not begin to accumulate before the abandonment
330 of T2, we use the offset of the T3/T2 riser, divided by the abandonment age of T2, to calculate the slip
331 rate. At Cuoia, the offsets have the same geometry with respect to the river as at Shengkang, but
332 we cannot use the same model, because the river geometries are different at these two sites. The
333 arc-shaped river at Cuoia has led to more erosion on the left side of the river (Figure 12e, f), so the
334 slip rate is obtained by dividing the offset of the T3/T2 riser by the abandonment age of T2.

335

336 Our results also place important constraints on the occurrence times of paleoearthquake events on
337 the southeastern segment of the Ganzi-Yushu fault. Our work demonstrates that two
338 paleoearthquake events are recorded in the trench at Renguo (Figure 13). We use OxCal 4.2.4
339 (Bronk Ramsey, 2009) to estimate the two events: event E1 (885-525 BC) and event E2
340 (7230-3015 BC). Based on our work on the Cuoia trench, there are also two paleoearthquake
341 events: event E1 (3580-2640 BC) and event E2 (2135-1510 BC). Considering that the distance

342 between Rengou and Cua is only 40 km and that there is no obvious step or discontinuity in the
343 fault trace over this distance, we suggest that the faults between Rengou and Cua are likely to have
344 similar rupture histories. If this is correct, then we can analyse earthquake occurrence times using
345 paleoearthquakes from the two trench sites and historical earthquakes. Two documented historical
346 earthquakes respectively occurred in 1320 AD and 1854 AD. Thus, while the data are limited,
347 there does seem to be some evidence of clustering of large earthquakes along the southeastern
348 Ganzi-Yushu fault (Figure 13). Three or four paleoearthquakes occurred during about 3000 years
349 from 3580-2640 BC to 885-525 BC (yielding an approximate recurrence interval of ~1000 a), but
350 there appear to have been no large earthquakes during the 2000 years from 885-525 BC to 1320
351 AD. Finally, two large historical earthquakes have happened in the past 630 years (Figure 13).
352 This apparent clustering behavior has been observed on other large strike-slip fault systems, for
353 example, Sieh [1989] discussed the clustering of earthquakes along the San Andreas Fault. Over
354 the Holocene at least, there is no evidence for periodic earthquakes on the southeastern
355 Ganzi-Yushu fault, and the occurrence of two large earthquakes since 1320 AD may indicate that
356 the fault is currently in a phase of relative activity.

357

358 **6 Conclusions**

359 We have documented Quaternary activity on the Ganzi-Yushu fault, using a combination of field
360 observations, photo and image interpretation, and trenching. The Ganzi-Yushu fault, which forms
361 part of the boundary between the Qiangtang and Bayankala blocks, has been active in the latest
362 Quaternary with an oblique sinistral-thrust sense of slip. More precise chronology and offset

363 measurements for the dominant sinistral strike-slip displacement suggest that sinistral strike-slip
364 rates may be 8-11mm/a. Apparent throw rates are typically ~1 mm/a. Our trench investigations
365 indicate that Holocene earthquakes on the southeastern segment of the Ganzi-Yushu fault show
366 some evidence for clustering of activity. From the past 5600 years, the fault appears to have
367 undergone two active periods separated by a period of relative quiescence. Our more precise slip
368 rates provide essential evidence in understanding the mechanism of the Bayan Har fault-block in
369 the India-Asia collision.

370

371 **Acknowledgements:**

372 This work has been funded by the central level, scientific research institutes for basic R & D
373 special fund business (IGCEA1416) and Yushu Earthquake Science Investigation of China
374 Earthquake Administration.

375

376 **References**

377 Allen C R, Luo Z, Qian H, et al (1991). Field study of a highly active zone: the Xianshuihe fault of southwestern
378 China. *Geol. Soc. Am. Bull.*, 103,1178-1199.

379 Avouac, J.-P., and P. Tapponnier (1993), Kinematic model of active deformation in central Asia, *Geophys. Res. Lett.*,
380 20, 895 – 898.

381 Bronk Ramsey, C. (2009). Bayesian analysis of radiocarbon dates. *Radiocarbon*, 51(1), 337-360.

382 Burchfiel, B. C., Z. Chen, Y. Liu, and L. H. Royden(1995), Tectonics of the Longmen Shan and adjacent regions,
383 *Int. Geol. Rev.*, 37, 661 – 735.

384 Chen, L.C., H., Wang, Y.K. Ran, X.-Z. Sun, G.W. Su, J. Wang, X.B. Tan, Z.M. Li, and X.Q. Zhang (2010), The
385 Ms7.1 Yushu earthquake surface rupture and large historical earthquakes on the Garzê-Yushu
386 Fault, *Chin. Sci. Bull.*, 55(31), 3504-3509.

387 Chen, S., C. J. L. Wilson, Q. Deng, X. Zhao, and Z. Luo (1994), Active faulting and block movement
388 associated with large earthquakes in the Min Shan and Longmen Mountains, northeastern Tibetan Plateau, *J.*
389 *Geophys. Res.*, 99, 24025 – 24038.

390 Chen, Y.T., 2010. The report of focal mechanism and rupture process of 2010. 4. 14 Yushu earthquake, Qinghai,
391 China (the fourth edition). [http://www.csi.ac.cn/manage/html/4028861611c5c2ba0111c5c558b00001/](http://www.csi.ac.cn/manage/html/4028861611c5c2ba0111c5c558b00001/_content/10_04/17/1271488288058.html)
392 [_content/10_04/17/1271488288058.html](http://www.csi.ac.cn/manage/html/4028861611c5c2ba0111c5c558b00001/_content/10_04/17/1271488288058.html) (in Chinese).

393 Clark, M. K., M. A. House, L. H. Royden, K. X. Whipple, B. C. Burchfiel, X. Zhang, and W. Tang (2005), Late
394 Cenozoic uplift of southeastern Tibet, *Geology*, 33, 525 – 528.

395 Cowgill, E. (2007), Impact of riser reconstructions on estimation of secular variation in rates of strike-slip faulting:
396 Revisiting the Cherchen River site along the Altyn Tagh Fault, NW China, *Earth Planet. Sci. Lett.*, 254, 239 -
397 255.

398 Densmore, A. L., M. A. Ellis, Y. Li, R. J. Zhou, G. S. Hancock, and N. Richardon (2007), Active tectonics of the
399 Beichuan and Pengguan faults at the eastern margin of the Tibetan Plateau, *Tectonics*, 26, TC4005,
400 doi:10.1029/2006TC001987.

401 Dewey, J. F., W.C. Pitman, W.B.F. Ryan, and J. Bonnin (1973), Plate tectonics and the evolution of the Alpine
402 system, *Geol. Soc. Am. Bull.*, 84, 3137-3180.

403 England, P., and D. McKenzie (1982), A thin viscous sheet model for continental deformation, *Geophys. J. R.*
404 *Astron. Soc.*, 70, 295 – 321.

405 England, P., and G. Houseman (1986), Finite strain calculations of continental deformation: 2. Comparison with the

406 India-Asia Collision, *J. Geophys. Res.*, *91*, 3664 – 3676.

407 England, P., and P. Molnar (2005), Late Quaternary todecadal velocity fields in Asia, *J. Geophys. Res.*, *110*, B12401,
408 doi:10.1029/2004JB003541.

409 Forman, S. L. (1989), Applications and limitations of thermoluminescence to date Quaternary sediments, *Quatern.*
410 *Int.*, *1*, 47-59.

411 Gan, W.J., P.Z. Zhang, Z.K. Shen, Z.J. Niu, M. Wang, Y.G. Wan, D.M. Zhou, and J. Cheng (2007), Present-day
412 crustal motion within the Tibetan Plateau inferred from GPS measurements, *J. Geophys. Res.*, *112*, B08416,
413 doi:10.1029/2005JB004120.

414 He, H.L., Ran, H.L., Ikada, Y.,(2006). Uniform strike-slip rate along the Xianshuihe-Xiaojiang fault system and its
415 implications for active tectonics in southeastern Tibet. *ACTA Geologica Sinica*, *2*: 376-386.

416 Kirby, E., K. X. Whipple, B. C. Burchfiel, W. Tang, G. Berger, Z. Sun, and Z. Chen (2000), Neotectonics of the Min
417 Shan, China: Implications for mechanisms driving Quaternary deformation along the eastern margin of the
418 Tibetan Plateau, *Bull. Geol. Soc. Am.*, *112*, 375 – 393.

419 Kirby, E., K. X. Whipple, W. Tang, and Z. Chen (2003), Distribution of active rock uplift along the eastern margin
420 of the Tibetan Plateau: Inferences from bedrock channel longitudinal profiles, *J. Geophys. Res.*, *108*(B4),
421 2217, doi:10.1029/2001JB000861.

422 Kirby, E., P. W. Reiners, M. A. Krol, K. X. Whipple, K. V. Hodges, K. A. Farley, W. Tang, and Z. Chen (2002), Late
423 Cenozoic evolution of the eastern margin of the Tibetan Plateau: Inferences from $^{40}\text{Ar}/^{39}\text{Ar}$ and (U-Th)/He
424 thermochronology, *Tectonics*, *21*(1), 1001, doi:10.1029/2000TC001246

425 Li, C.-Y., J.-Z. Pang, and Z.-Q. Zhang (2012), Characteristics, geometry, and segmentation of the surface rupture
426 associated with the 14 April 2010 Yushu earthquake, eastern Tibet, China, *Bull. Geol. Soc. Am.*, *102*(4),
427 1618-1638.

428 Li, M.F, C.Q.Xing, C.X.Cai, W.X.Guo, S.X.Wu, Z.Z.Yuan, Y.Q.Meng, D.L.Tu, R.B.Zhang and R.J. Zhou (1995),
429 Research on activity of Yushu fault. *Seismology and Geology*, 17(3): 218-224 (in Chinese with English
430 abstract).

431 McCalpin, J.P. (1996),Paleoseismology. Elsevier, New York.

432 Meade, B. J. (2007), Present-day kinematics at the India-Asia collision zone, *Geology*, 35, 81 – 84.

433 Mériaux, A. S., F. J. Ryerson, P. Tapponnier, J. van derWoerd, R. C. Finkel, X. Xu, Z. Xu, and M. W.Caffee (2004),
434 Rapid slip along the central AltynTagh Fault: Morphochronologic evidence fromCherchen He and
435 SulamuTagh, *J. Geophys. Res.*, 109, B06401, doi:10.1029/2003JB002558.

436 Molnar, P., and P. Tapponnier (1975), Cenozoic tectonicsof Asia: Effects of a continental collision,*Science*, 189,
437 419 -426.

438 Molnar, P., and P. Tapponnier (1978), Active tectonics of Tibet, *J. Geophys. Res.*, 83, 5361-5375.

439 Peltzer, G., and F. Saucier (1996), Present-day kinematics of Asia derived from geological fault rates,*J. Geophys.*
440 *Res.*, 101, 27,943 - 27,956.

441 Peng, H., Ma, X.M., Bai, J.Q., Du, D.P., (2006). Characteristics of quaternary activities of the Ganzê-Yushu fault
442 zone. *Journal of Geomechanics*, 12(3): 295-304.

443 Seih, K., M. Stuiver and D. Brillinger (1989), A more precise chronology of earthquakes produced by the San
444 Andreas Fault in southern California. *J. Geophys. Res.*, 94,603-623.

445 Shen, Z.K., J.N. Lü, M. Wang, and R. Bürgmann(2005), Contemporary crustal deformation aroundthe southeast
446 borderland of the Tibetan Plateau,*J. Geophys. Res.*, 110, B11409, doi:10.1029/2004JB003421.

447 Tapponnier, P., Z.Q. Xu, F. Roger, B. Meyer, N. Arnaud,G.Wittlinger, and J.-S. Yang (2001), Oblique stepwiserise
448 and growth of the Tibet Plateau, *Science*, 294,1671-1677.

449 Thatcher, W. (2007), Microplate model for the present-daydeformation of Tibet, *J. Geophys. Res.*, 112,B01401,

450 doi:10.1029/2005JB004244.

451 USGS. (2010), Magnitude 6.9 Southern Qihai, China.<http://earthquake.usgs.gov/earthquakes/recenteqsww>

452 /Quakes/us2010vacp.php

453 Van der Woerd J P, Tapponnier F J, Ryerson, et al. (2002). Uniform postglacial slip-rate along the central 600 km

454 of the Kunlun Fault (Tibet), from ²⁶Al, ¹⁰Be, and ¹⁴C dating of riser offsets, and climatic origin of the

455 regional morphology. *Geophys. J. Int.*, 148, 356-388.

456 Wang, Q., P.Z. Zhang, J. T. Freymuller, R. Bilham, K. M. Larson, X.-A. Lai, X.-Z. You, Z.-J. Niu, J.-C. Wu, Y.-X.

457 Li, J.-N. Liu, Z.-Q. Yang, and Q.-Z. Chen (2001), Present-day crustal deformation in China constrained by

458 global positioning system measurements, *Science*, 294, 574-577.

459 Wang, Y. Z. (2009). Continental Deformation Models and Their Application to Eastern Tibetan Plateau, *Doctoral*

460 *dissertation* , Institute of Geology, China Earthquake Administration, Beijing.

461 Wen, X.Z, Xu, X.W., Zheng, R.Z., Xie, Y.Q., Wan, C., (2003). Average slip-rate and recent large earthquake

462 ruptures along the Garzê-Yushu fault. *Science in China (Series D)*, 46(Suppl): 276-288.

463 Xu, G., and P. J. J. Kamp (2000), Tectonics and denudation adjacent to the Xianshuihe fault, eastern Tibetan Plateau:

464 Constraints from fission track thermochronology, *J. Geophys. Res.*, 105, 19231 – 19251.

465 Xu, X.W., X.B. Tan, G.D. Wu, J.B. Chen, J. Shen, W. Fang, and H.P. Song. (2011). Surface rupture features of the

466 2008 Yutian Ms7.3 earthquake and its tectonic nature. *Seismology and Geology*, 33(2): 462-471.

467 Xu, X.W. (2000), Scientific investigation of Mani earthquake in the north Tibet, in *Yearbook of China Earthquake*

468 *Research*, pp.327-329, China Earthquake Press, Beijing.

469 Xu, X.W., W.B. Chen, W.T. Ma, G.H., Yu and G.H. Chen. (2002). Surface rupture of the Kunlunshan earthquake

470 (Ms8.1), northern Tibetan Plateau, China. *Seismological Research Letters*. 73(6): 884-892.

471 Xu, X.W., X.Z Wen, G.H. Yu, G.H. Chen, Y. Klinger, J. Hubbard and J. Shaw. (2009). Coseismic revers- and

472 oblique-slip surface faulting generated by the 2008 Mw7.9 Wenchuan earthquake, China. *Geology*, 37(6):
473 515-518.

474 Zhang, P.Z., Q.D.Deng, G.M.Zhang (2003),Active tectonics blocks and strong earthquakes in the continent of
475 China. *Science in China (Series D)*, 46(Suppl): 13-24.

476 Zhang, P.Z., et al. (2004), Continuous deformation ofthe Tibetan Plateau from global positioning systemdata,
477 *Geology*, 32, 809-812.

478 Zhou, R.J., S.H.Ma , C.X.Cai (1996), Late Quaternary active features of the Ganzi-Yushu fault zone. *Earthquake*
479 *Research in China*, 12(4): 250-260.

480 Zhou, R. J., X. Z. Wen, C. X. Chai, S. H. Ma (1997), Recent earthquakes and assessment of seismic tendency on
481 the Ganzi-Yushu fault zone. *Seismology and Geology*, 19(2): 115-124.

482

483 **Figure captions**

484 **Figure 1.** Regional seismotectonics and historical earthquakes of the study region. A, Simplified
485 map of major tectonic boundaries and Tertiary faults in Tibet (after [Tapponnier et al., 2001](#)). Bold
486 black lines are major faults and localized shear zones (megathrust or strike-slip) with largest finite
487 offsets, dashed where uncertain. Thin red lines are crustal thrusts. Red circles are the four largest
488 earthquakes ($M_w > 7.0$) during the last two decades in Tibet. Pentagram is the 2010 M_w 6.9 Yushu
489 earthquake. The black rectangle indicates the location of panel B. B, faults, major river systems,
490 and areas of Quaternary deposition in the east-central Tibetan Plateau. The fault locationsare
491 modified from Deng [[2007](#)].The 2010 Yushu earthquake focal mechanism was extracted from the
492 CDSN [[Chen, 2010](#)], USGS and Harvard [[USGS, 2010](#)] catalogues.

493

494 **Figure 2.** A, historical earthquake surface ruptures along the Ganzi-Yushu fault. Surface ruptures
495 of the 2010 M_w 6.9 Yushu earthquake from Chen et al. [2010] and Li et al. [2012]. Surface
496 ruptures of the 1896, 1866 and 1854 earthquakes from Wen et al. [2003]. B, strike-slip rates along
497 the Ganzi-Yushu fault. Black, blue and purple circles are geological estimates of strike-slip rates
498 from Zhou et al. [1996], Wen et al. [2003] and Peng et al. [2006], respectively. Black, white, red
499 and blue lines with shadows are strike-slip rates and errors estimated from GPS surveys[Wang et
500 al., 2001; Shen et al., 2005; Gan et al., 2007; Wang, 2009]

501

502 **Figure 3.** Map of offset fill terraces at Shengkang. A, the original stereoscopic pair aerial
503 photograph. B, geomorphic interpretation of the aerial photograph. Yellow, green and brown areas
504 are T3, T4 and T5 surfaces. Blue area is the present-day river. Red square is the location of the TL
505 age sample from Wen et al. [2003]. Black line is the location of topographic profile in C. C,
506 topographic profile extracted from a 20 m DEM constructed from 1:50,000 maps.

507

508 **Figure 4.** Tectonic landforms and evidence of fault activity at Renguo. A, the original aerial
509 photograph. B, interpreted photograph showing the locations of panels C-F. C, oblique photograph
510 of the fault scarp; see the location in panel B. View to south. The location of the Renguo trenches
511 is shown in yellow. D, oblique photograph of the sag pond. Dashed red lines show the uncertain
512 fault trace; see the location in panel B. View to southwest. E, contour map near the trench (0.2 m
513 contour interval), obtained from a differential GPS measuring system. The fault scarp is about
514 1-1.5 m high; see the location in panel B. F, displacement of the footpath in Ezhong village. View

515 to south; see the location in panel B.

516

517 **Figure 5.** Trench site on the Ganzi-Yushu fault at Renguo. See figure 4 for location. A, log of west
518 wall of Renguo trench 1 (RGTC1). B, log of east wall of RGTC1. C, log of south wall of Renguo
519 trench 2 (RGTC2). D, log of north wall of RGTC2. Black lines separate units 1-4. See Table 1 for
520 description of units. Faults F1-F4 are shown by red lines. Black triangles show locations of ¹⁴C
521 samples. Calibrated ages and sample numbers (Table 2) are shown in bold type. E, sketch map of
522 U3 offsets. Grey area is U3, yellow area is the fault zone.

523

524 **Figure 6.** Results of OxCal analysis of radiocarbon dates from the trenching site. Lines with
525 no fill are prior probability distributions, and solid curves are posterior distributions after OxCal
526 analysis. Phases are summed probability for units with multiple radiocarbon dates.

527

528 **Figure 7.** Evidence for fault activity at Cuoqa. A, the original stereoscopic pair aerial photograph.
529 B, geomorphic interpretation of aerial photograph. Yellow to pale green shades represent T0-T3
530 terrace surfaces. Black rectangle is the location of trench. Red line indicates the fault traces.
531 Dashed white lines indicate the T3/T2 riser, which is offset sinistrally by ~80m. C, overview of the
532 site, looking northwest. See location and orientation in panel B. D, close-up photograph of the
533 fault exposed in the T2/T0 riser. Bold red line is the fault, and yellow line is the top of Triassic
534 bedrock. Fault dip direction and dip angle are shown in bold type.

535

536 **Figure 8.** Trench site on the Ganzi-Yushu fault at Cuoqa. See Figure 7 for location. A, photo of

537 west wall of Cuoia trench 1 (CATC1). B, log of west wall of Cuoia trench 1 (CATC1). C, photo of
538 east wall of Cuoia trench 1 (CATC1). D, log of east wall of CATC1. Black lines separate units 1-5.
539 See Table 3 for description of units. Faults F1-F5 shown by red lines. Black triangles show
540 locations of ^{14}C samples. Calibration ages and sample numbers are shown in bold type.

541

542 **Figure 9.** Results of OxCal analysis of radiocarbon dates from the trenching site. Lines with
543 no fill are prior probability distributions, and solid curves are posterior distributions after OxCal
544 analysis. Phases are summed probability for units with multiple radiocarbon dates.

545

546 **Figure 10.** Interpretation of paleoearthquakes in the CATC1 trench. A, the original status of the
547 trench. B, the status after the first event. C, the status before the second event. D, the status after
548 the second event. E, the present status of the trench. Colors represent different units. Black lines
549 separate units 1-5. See Table 3 for description of units. Faults F1-F5 shown by red lines.

550

551 **Figure 11.** Evidence for fault activity at Ria. A, aerial photograph of the fault trace and offset fill
552 terraces. B, interpreted photograph showing the terrace treads and the fault trace (red line). Dashed
553 white lines are the terrace risers. Offsets of the risers are shown in white bold type..

554

555 **Figure 12.** Possible terrace evolution models at the different sites discussed in this paper. A, the
556 original landscape at Shengkang. B, the present-day landscape at Shengkang. Red box indicates
557 the location of the measured riser offset. C, the original landscape at Ria. D, the present-day
558 landscape at Ria. Grey box is the eroded part of the upper terrace, which reduces the preserved

559 riser offset. Tan box is a part of the upper terrace which may also be eroded. E, the original
560 landscape at Cuoia. F, the present-day landscape at Cuoia. Note the arcuate path of the river and
561 erosion of the terrace riser on the right and left banks.

562

563 **Figure 13.** Occurrence times of pre-historical (black with arrows) and historical (dark grey)
564 earthquakes, and inferred active periods (light grey shading) of the southeastern segment of the
565 Ganzi-Yushu fault. The AD1320 event of Cuoia is inferred, because we lack direct
566 paleoseismological evidence of the earthquake at that site.

567

Table 1.Lithologic Units in RenguoTrench

| Unit | Description |
|---------|---|
| U1-1 | Grey-yellow coarse gravel layer, dominated by gravel and cobbles with a diameter of 5-20 cm, with rare clasts over 20 cm. The gravel is poorly sorted and is slightly rounded. In some areas the stratum is dark grey when freshly exposed and becomes grey-white when dry. |
| U1-2 | Grey gravel layer. The mean clast diameter is about 5 cm, with rare clasts over 10 cm. |
| U2 | Grey fine gravel layer with darker color than U1-2. The mean clast diameter is 1-3 cm. |
| U3 | Grey to brown fine gravel layer, with mean clast size of 5cm. This stratum in the west wall of RGTC1 is darker than the east. It only appears in the hanging wall of the east wall of RGTC1. The stratum thins from west to east in RGTC2. |
| U4-1 | Yellow clay layer (cultural layer). The stratum has low gravel content and the mean gravel diameter is 3cm. A lot of charcoal derived from burned straw is distributed within this layer. |
| U4-2 | Brown sandy clay layer which forms the surface soil and subsoil. The layer contains rare gravel clasts with diameter of 1-3cm. |
| Wedge A | Grey gravel layer. The mean clast diameter is about 5 cm, with rare clasts over 10cm. Materials in the wedge are similar to those from U1-1, but more loose. |
| Wedge B | Grey gravel layer. The mean clast diameter is about 10 cm, with rare clasts over 20 cm. There is obvious human remodeling in this layer. Materials in the wedge are similar to those from U4-1, but are coarser-grained. |

Table 2. Radiocarbon Samples and Analytical Results

| Sample | Material | Radiocarbon Age | $^{13}\text{C}/^{12}\text{C}$ Ratio | 2σ Calendar Age |
|-----------|----------|-------------------|-------------------------------------|---|
| CATC1-E3 | Charcoal | 3710 \pm 40 BP | -23.8‰ | 2270-2255 BC (0.8%) 2210-1975 BC (94.6%) |
| CATC1-E4 | Charcoal | 7160 \pm 50 BP | -23.9‰ | 6205-6190 BC (1.1%) 6185-6140 BC (2.8%) 6115-5970 BC (85.9%) 5955-5915 BC (5.6%) |
| CATC1-E5 | Charcoal | 3250 \pm 40 BP | -24.3‰ | 1620-1435 BC |
| CATC1-W3 | Charcoal | 4090 \pm 40 BP | -24.2‰ | 2870-2800 BC (19.3%) 2780-2560 BC (69.2%) 2535-2490 BC (6.9%) |
| CATC1-W4 | Charcoal | 4790 \pm 40 BP | -24.5‰ | 3655-3515 BC (92.7%) 3410-3405 BC (0.5%) 3400-3380 BC (2.2%) |
| CATC1-W6 | Charcoal | 830 \pm 40 BP | -24.8‰ | 1050-1085 AD (4.3%) 1150-1275 AD (91.1%) |
| RGTC1-E1 | Charcoal | 2470 \pm 30 BP | -23.0‰ | 770-475 BC (92.4%) 465-450 BC (1.2%) 445-430 BC (1.8%) |
| RGTC1-E14 | Charcoal | 990 \pm 40 BP | -23.2‰ | 985-1155 AD |
| RGTC1-E15 | Charcoal | 1030 \pm 30 BP | -22.2‰ | 900-920 AD (2.8%) 960-1045 AD (91.9%) 1105-1120 AD (0.7%) |
| RGTC1-E16 | Charcoal | 13390 \pm 50 BP | -25.3‰ | 14340-13960 BC |
| RGTC1-E17 | Charcoal | 8310 \pm 40 BP | -23.7‰ | 7500-7250 BC (90.5%) 7230-7190 BC (4.8%) |
| RGTC1-W6 | Charcoal | 960 \pm 30 BP | -24.4‰ | 1020-1155 AD |
| RGTC1-W9 | Charcoal | 2670 \pm 40 BP | -21.4‰ | 905-795 BC |
| RGTC2-N1 | Charcoal | 2710 \pm 40 BP | -21.6‰ | 930-800 BC |
| RGTC2-S2 | Charcoal | 3450 \pm 40 BP | -22.1‰ | 1885-1665 BC |
| RGTC1-W16 | Charcoal | 4330 \pm 40 BP | -21.9‰ | 3085-3065 BC (3.4%) 3030-2885 BC (92.0%) |

Note: All sample preparation and analyses were done by Beta Analytic Inc. All samples were analyzed using accelerator mass spectrometry. All of raw radiocarbon ages are calibrated by OxCal 4.2.4 (Bronk Ramsey, 2009). The calibration calculates probability distributions for raw radiocarbon ages with associated uncertainties (reported by the lab facility). Radiocarbon ages BP relative to 1950. All samples typically undergo the acid-alkali-acid (AAA) method before radiocarbon dating.

Table 3.Lithologic Units in Cuoia Trench

| Unit | Description |
|---------|---|
| U1 | Cyan upper Triassic metasandstone. |
| U2 | Brown coarse gravel layer, with some clay in the matrix. The mean gravel diameter is about 10-20 cm, with some finer grains of 2-5 cm. |
| U3 | Black clay layer, with some fine gravel and mica fragments. The mean grain size of the gravel is 2-3 cm, with rare grains to 10 cm. |
| U4 | Brown clay layer, with some fine gravel with a diameter of 1-2 cm. |
| U5 | Brown clay layer (surface layer), with some fine gravel. The diameter of the gravel is about 2-5 cm. |
| Wedge A | Grey clay wedge. The wedge contains some fine gravel with a mean diameter of about 2-3 cm. Materials in the wedge were similar to those from U3. |
| Wedge B | Light brown clay and fine gravel wedge. The grain size of the fine gravel is 3-5 cm. Materials in the wedge were very similar to those in U5. |

Figure1

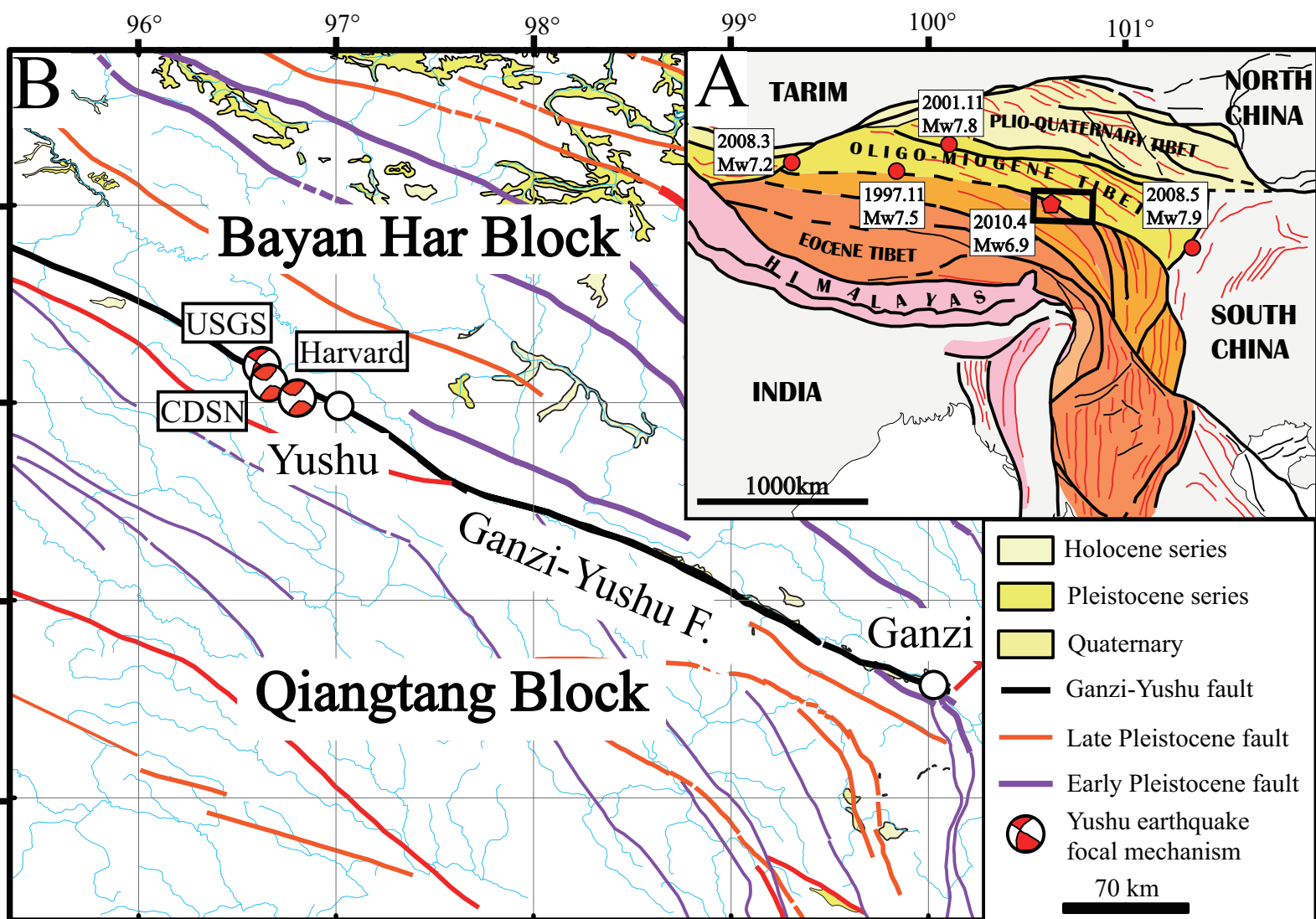


Figure2

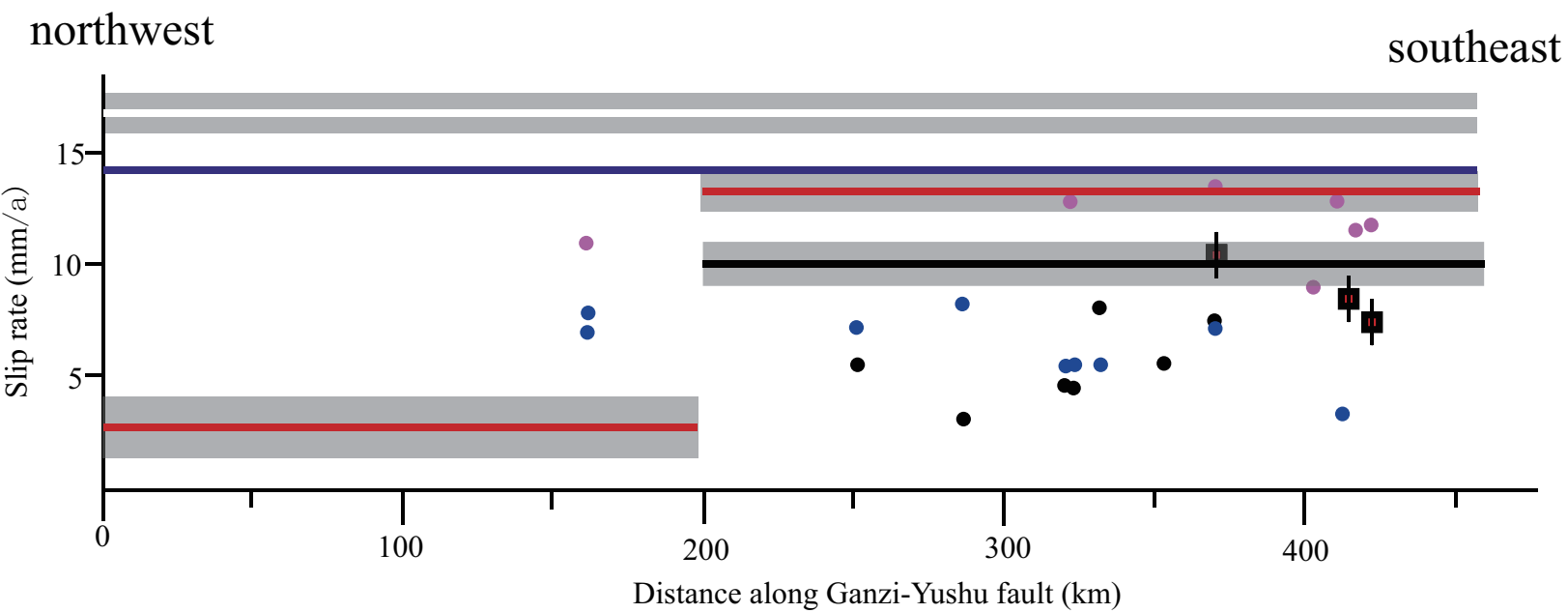
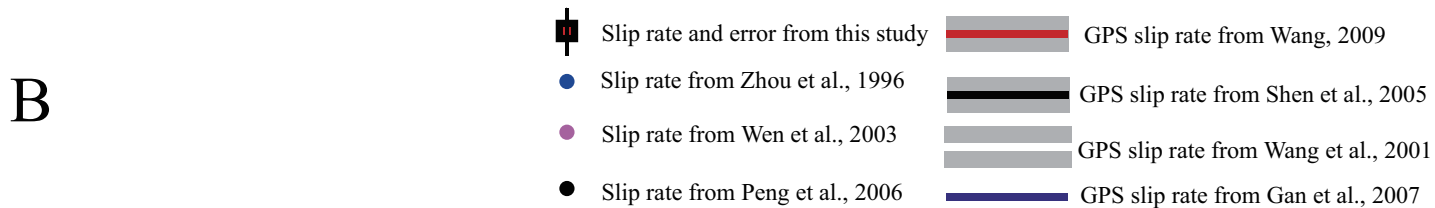
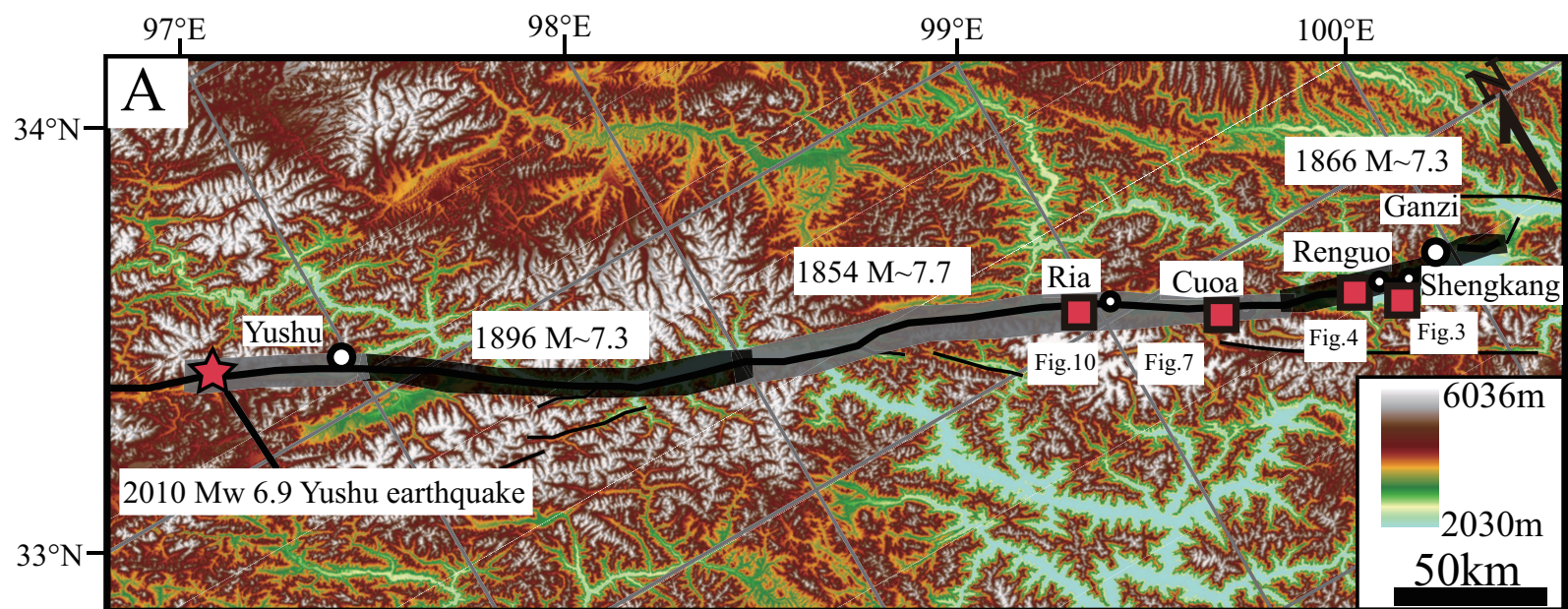
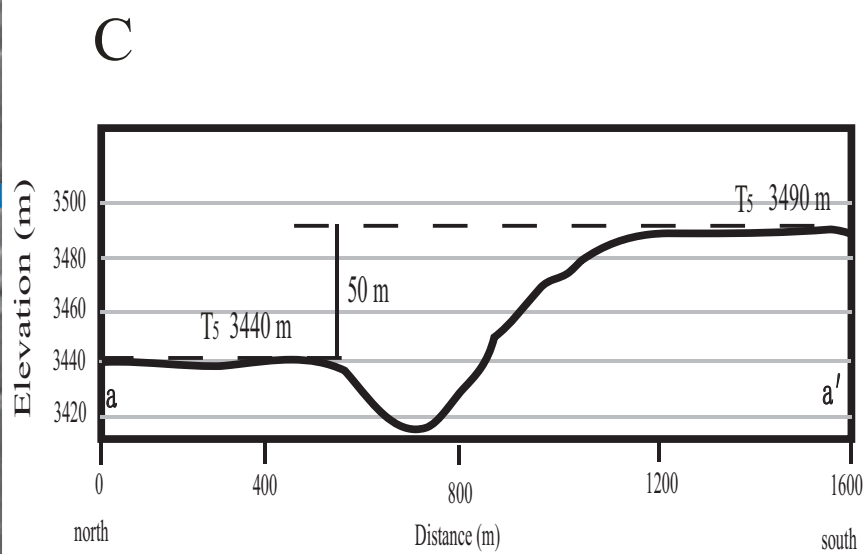
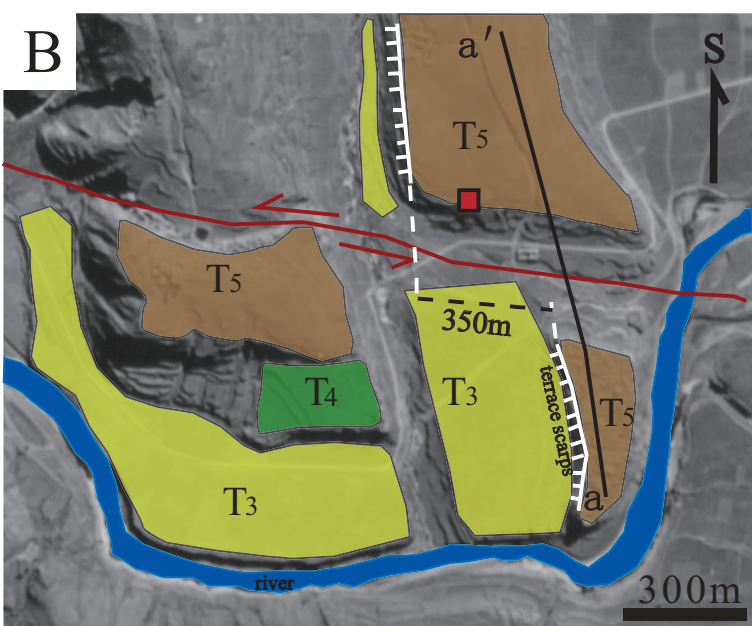
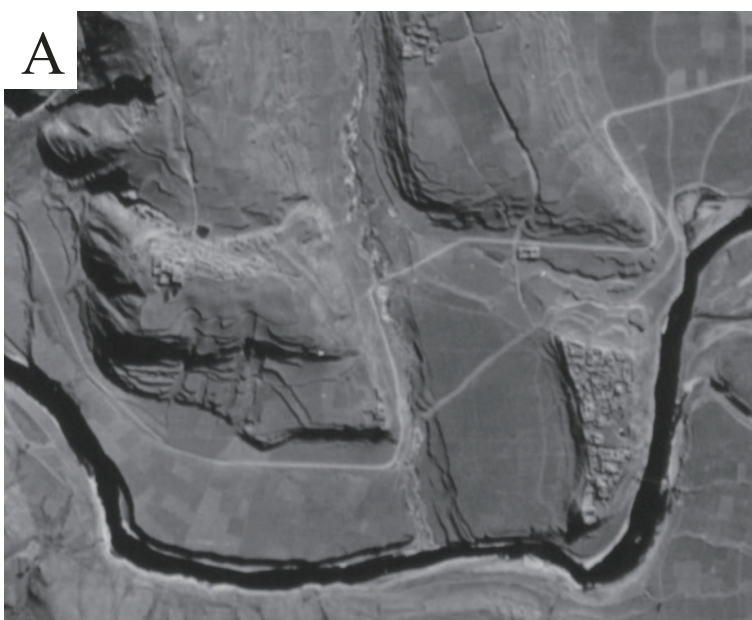


Figure3



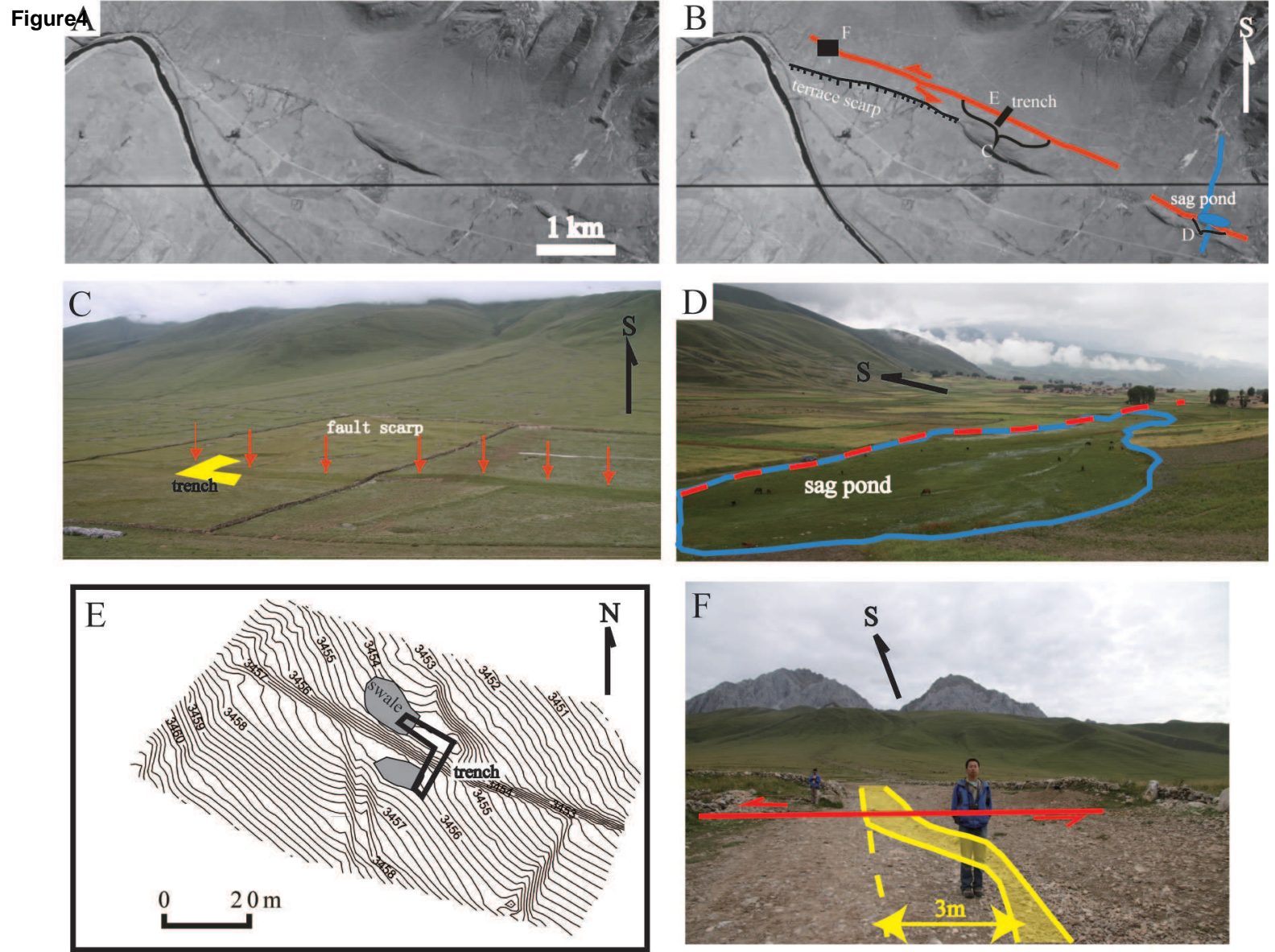


Figure 4. Tectonic landforms and evidence of fault activity at Renguo. A, the original aerial photograph. B, interpreted photograph showing the locations of panels C-F. C, oblique photograph of the fault scarp; see the location in panel B. View to south. The location of the Renguo trenches is shown in yellow. D, oblique photograph of the sag pond. Dashed red lines show the uncertain fault trace; see the location in panel B. View to southwest. E, contour map near the trench (0.2 m contour interval), obtained from a differential GPS measuring system. The fault scarp is about 1-1.5 m high; see the location in panel B. F, displacement of the footpath in Ezhong village. View to south; see the location in panel B.

Figure 5

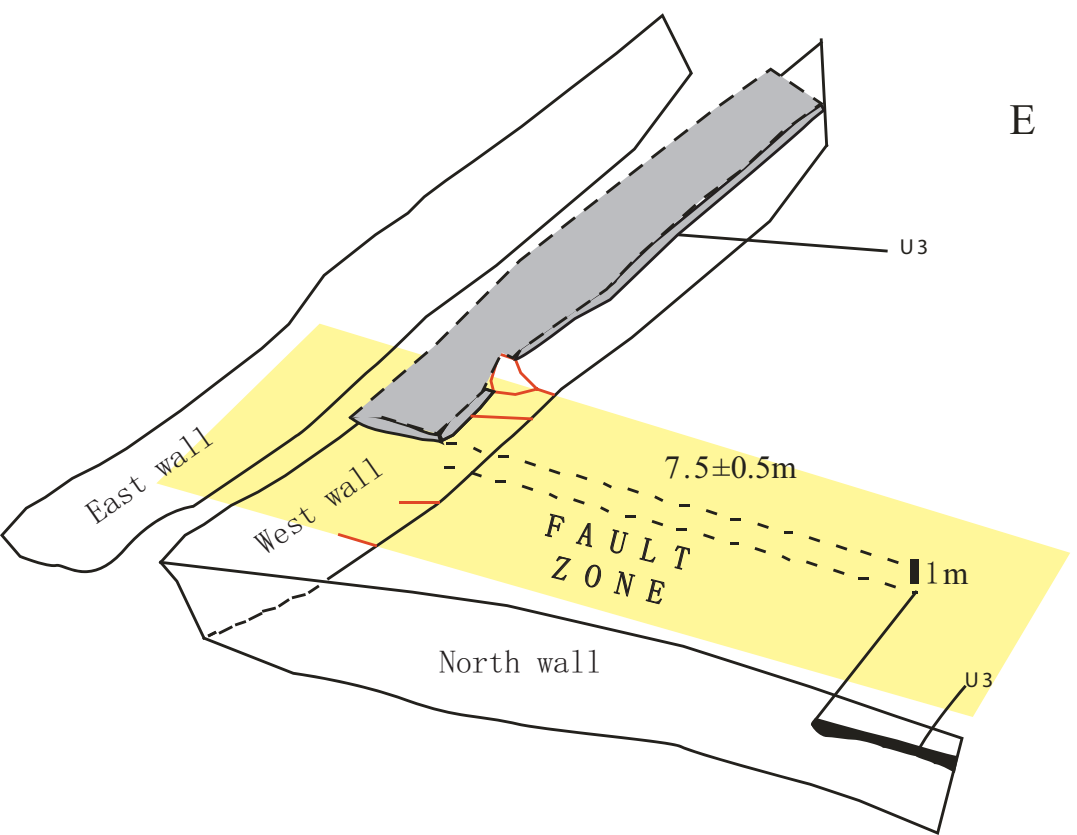
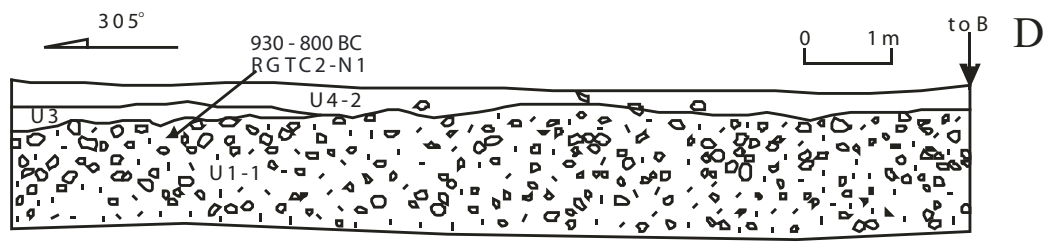
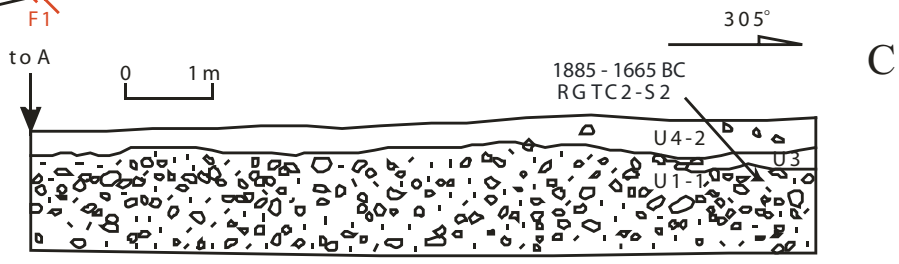
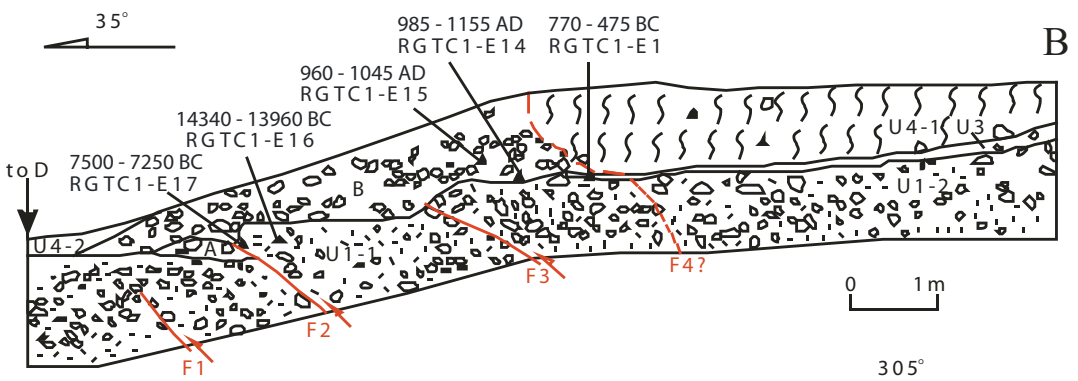
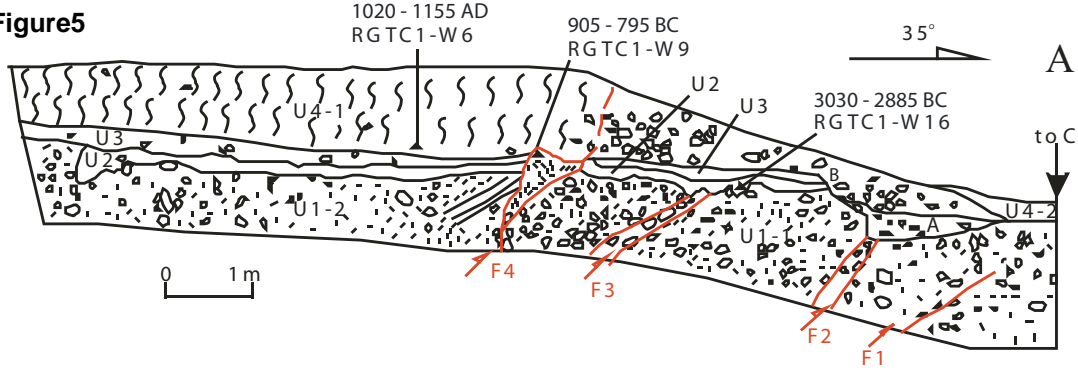


Figure6

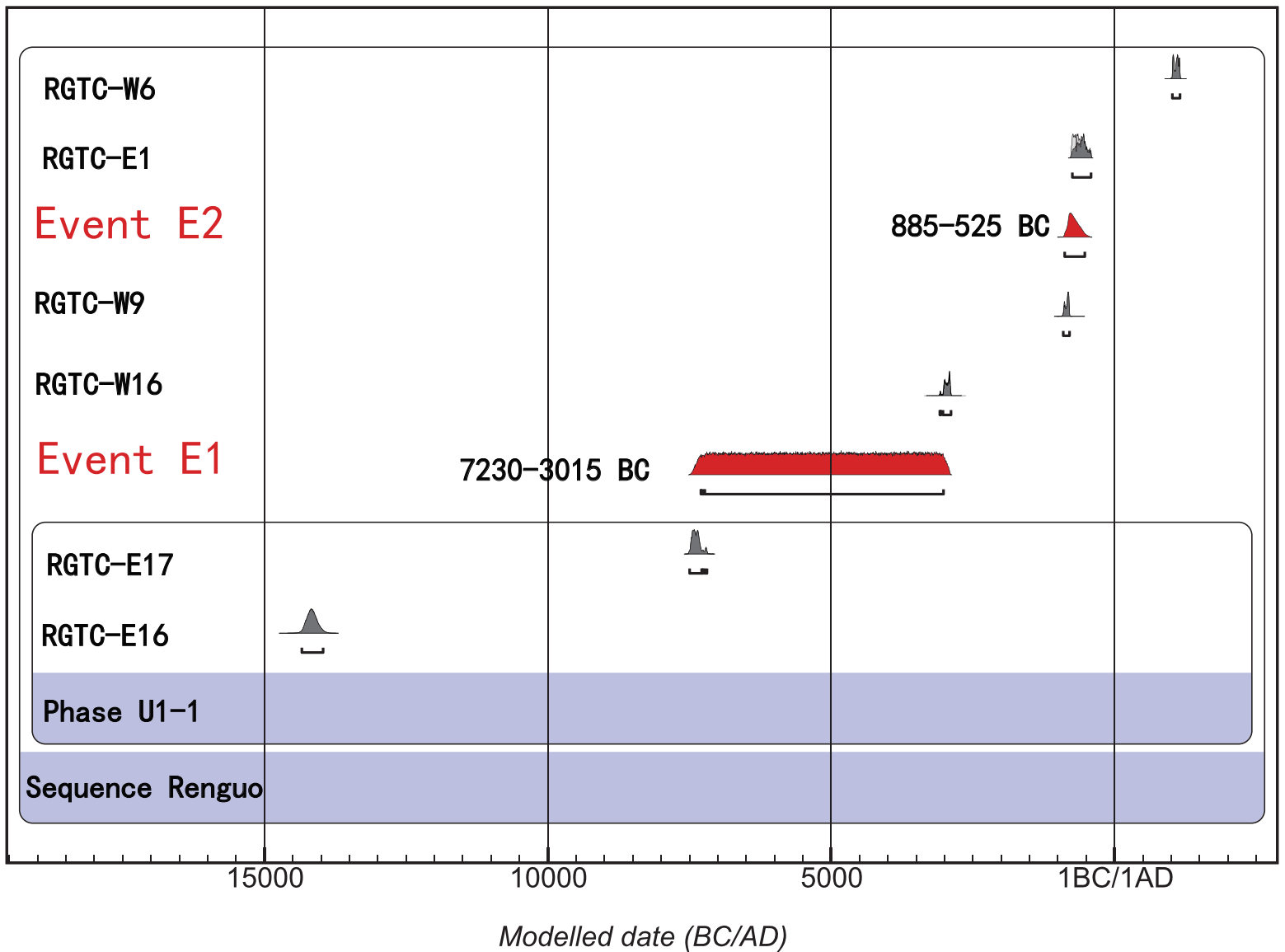


Figure7

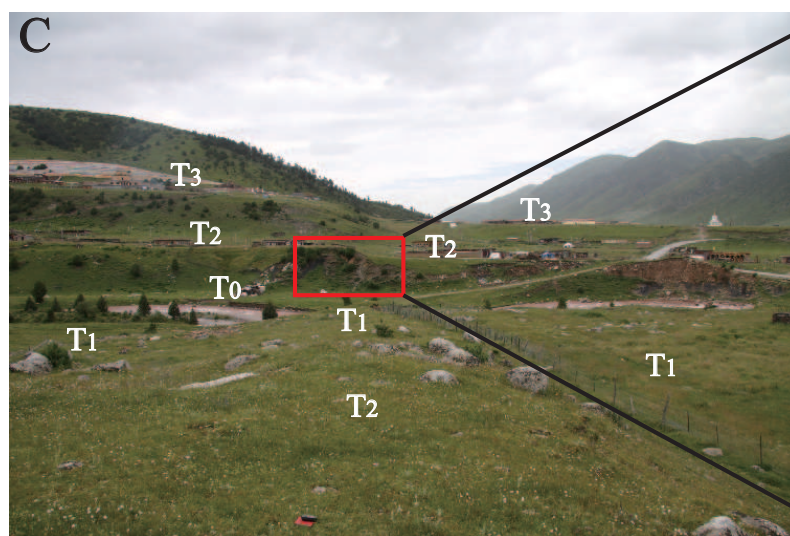
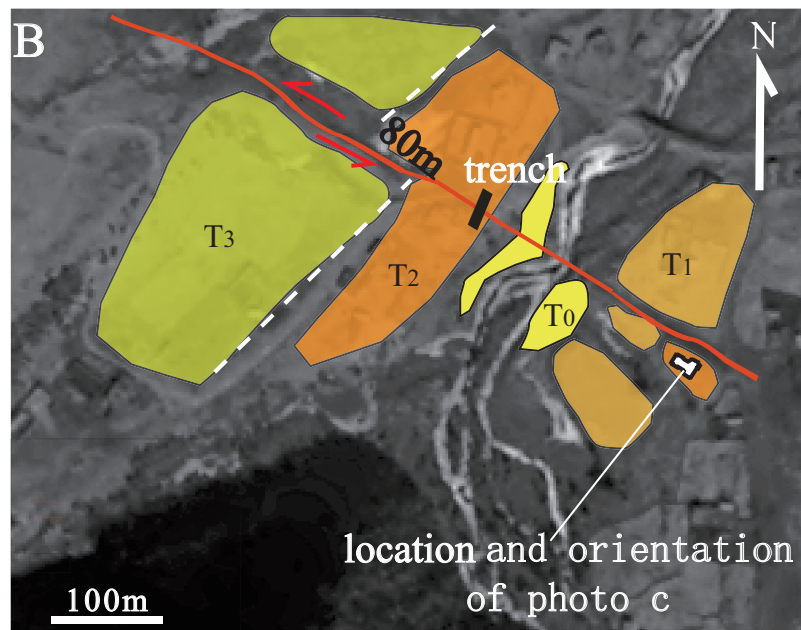
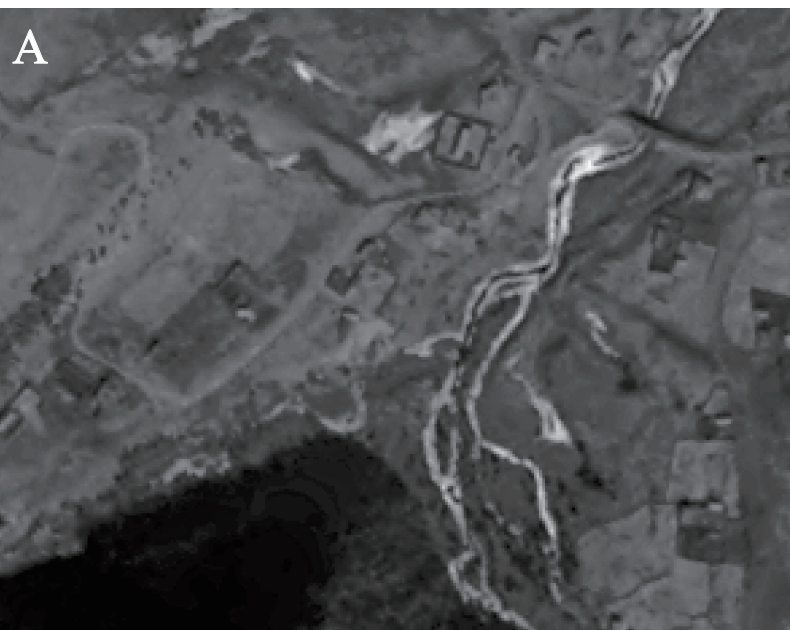


Figure 8

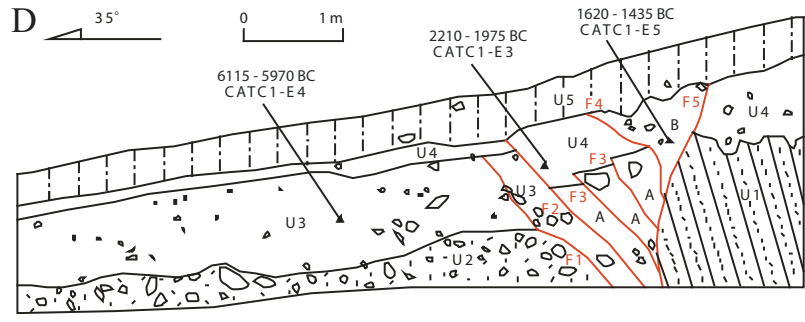
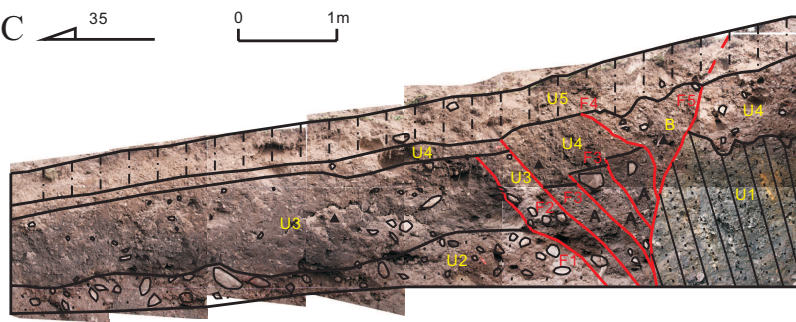
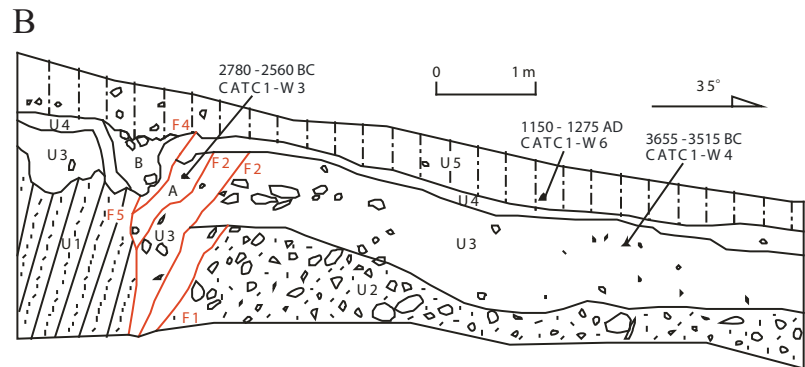
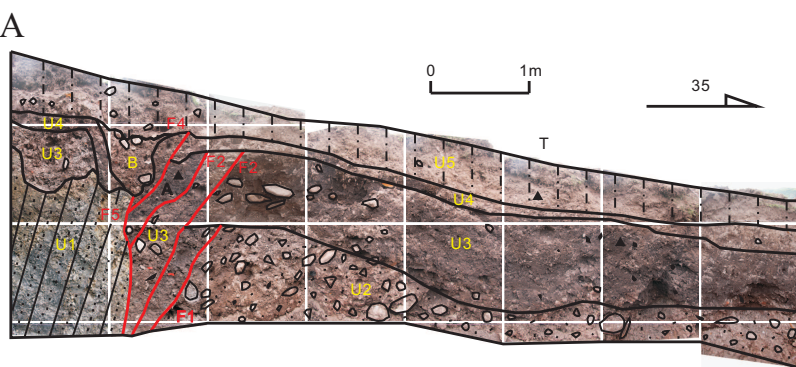


Figure9

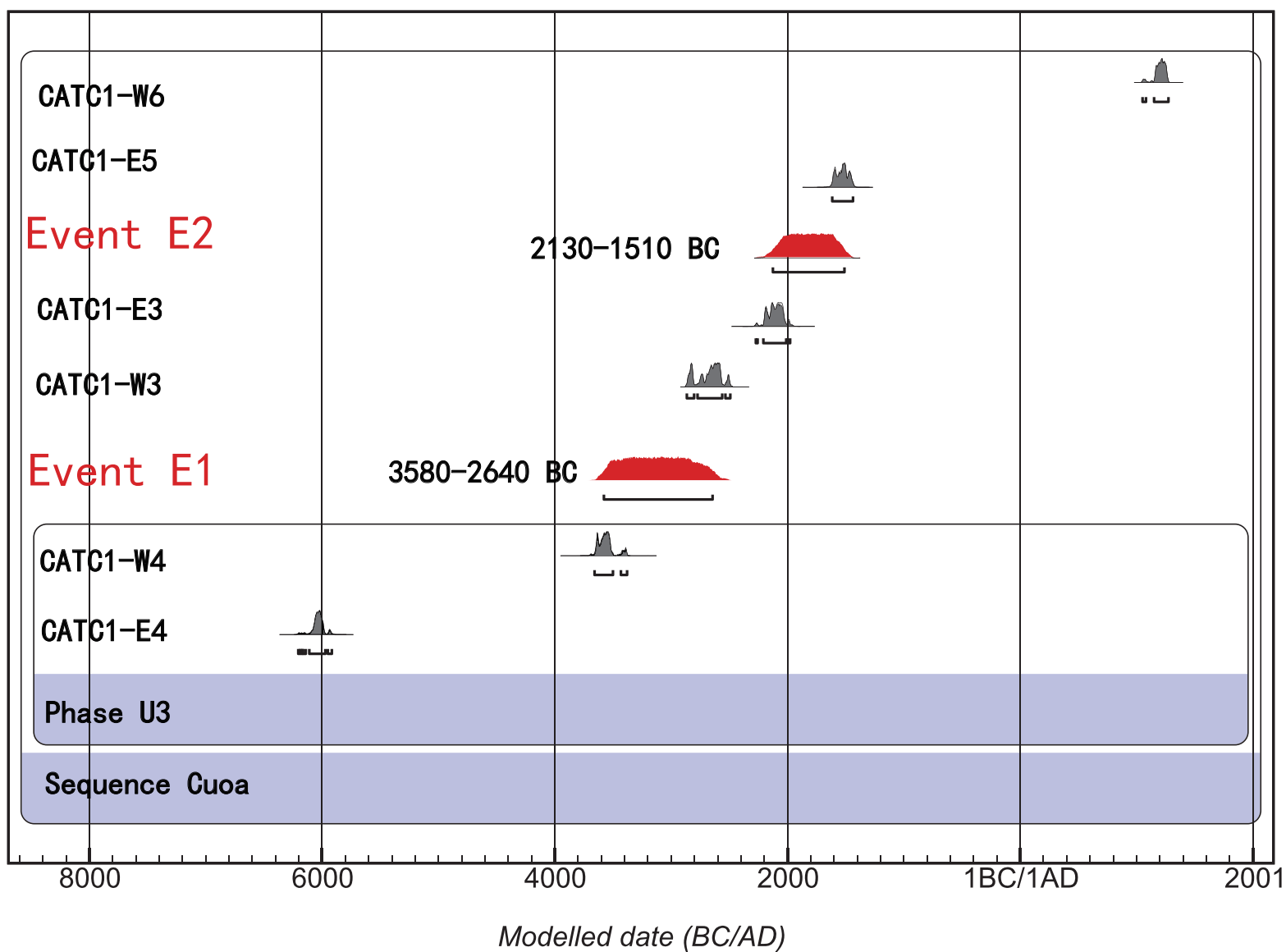


Figure10

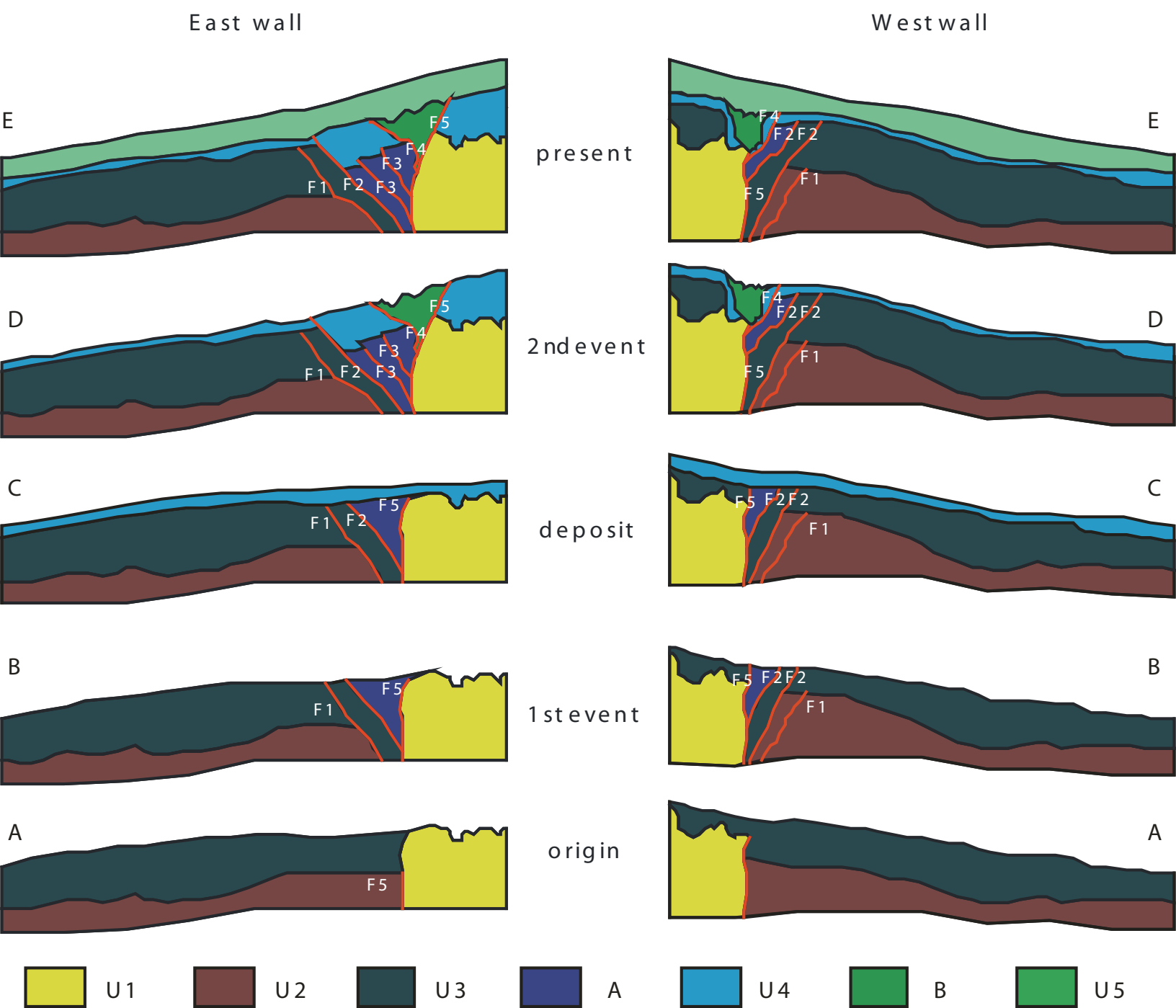


Figure11

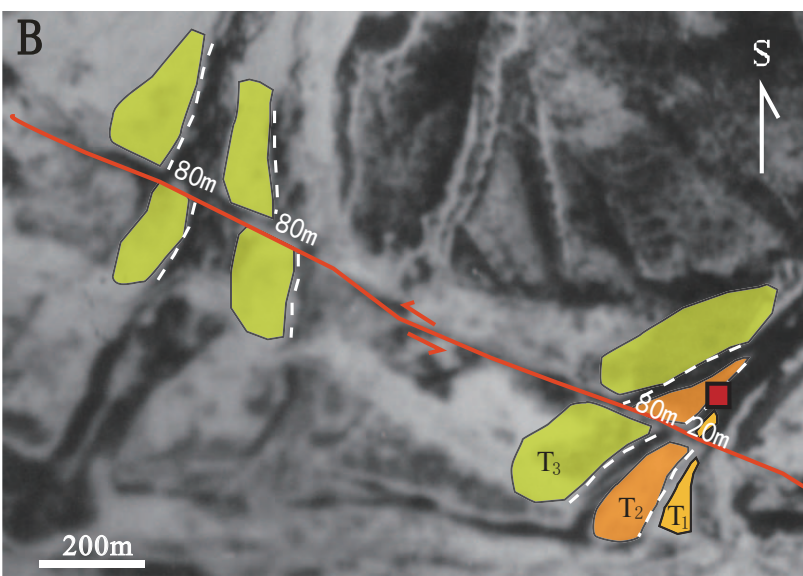
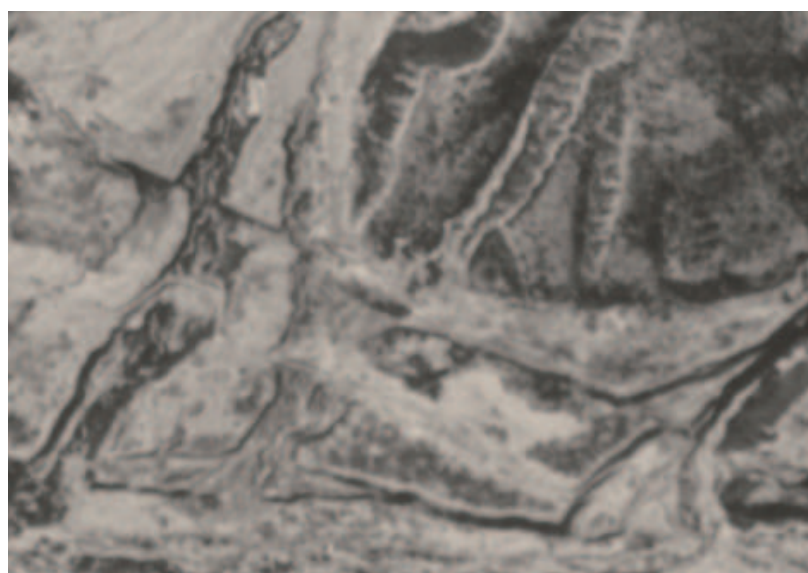
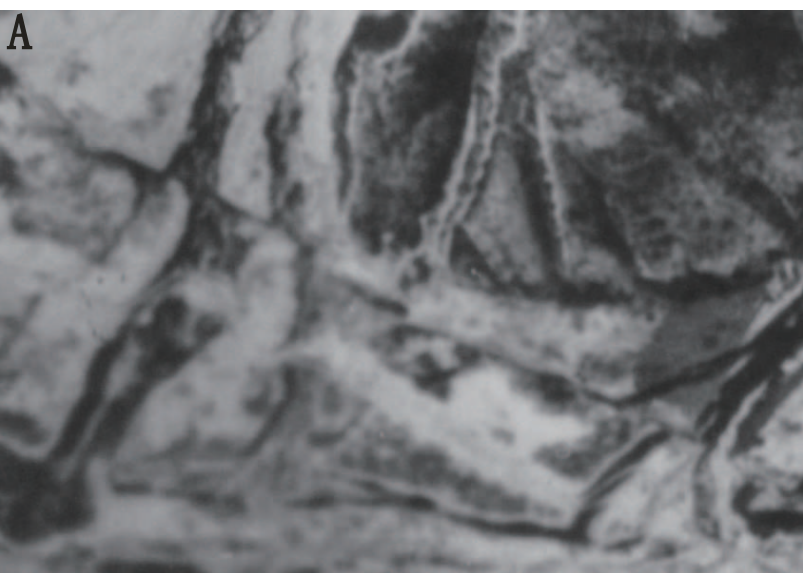
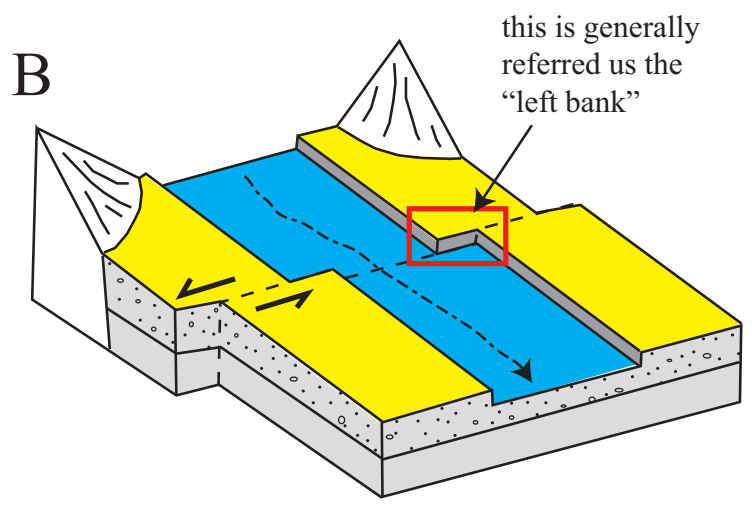
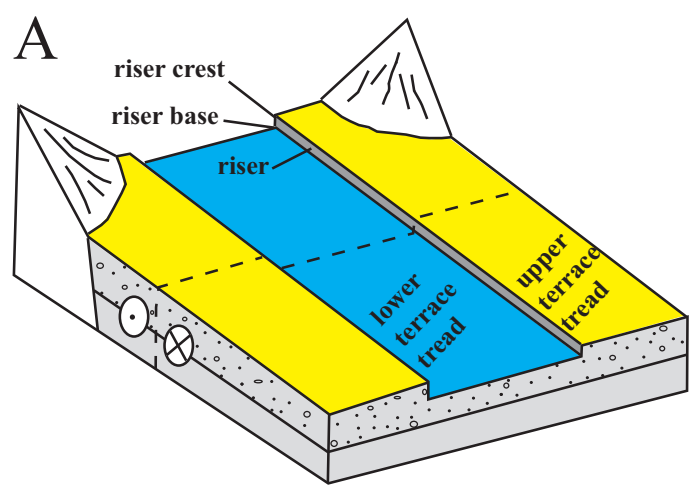
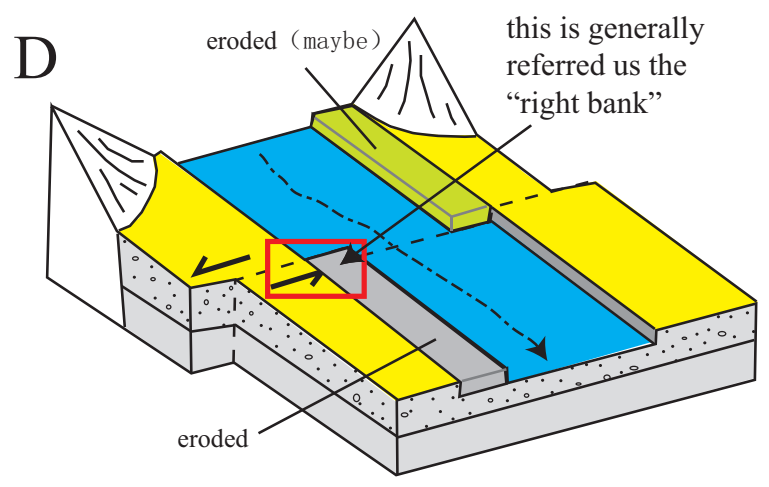
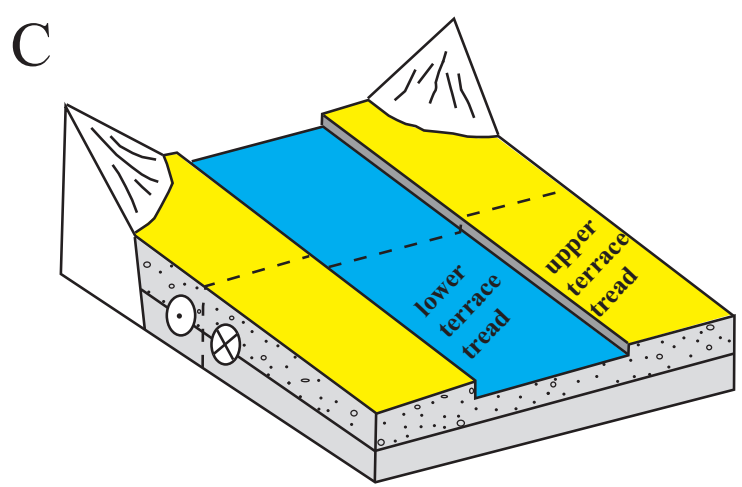


Figure12

Shengkang



Ria



Cuoia

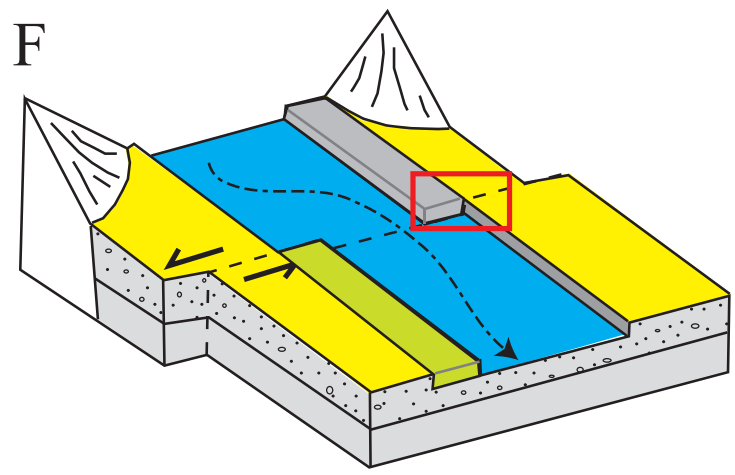
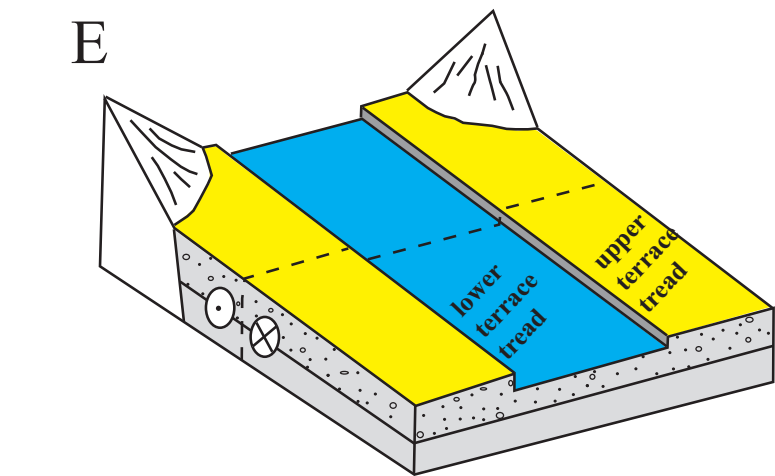
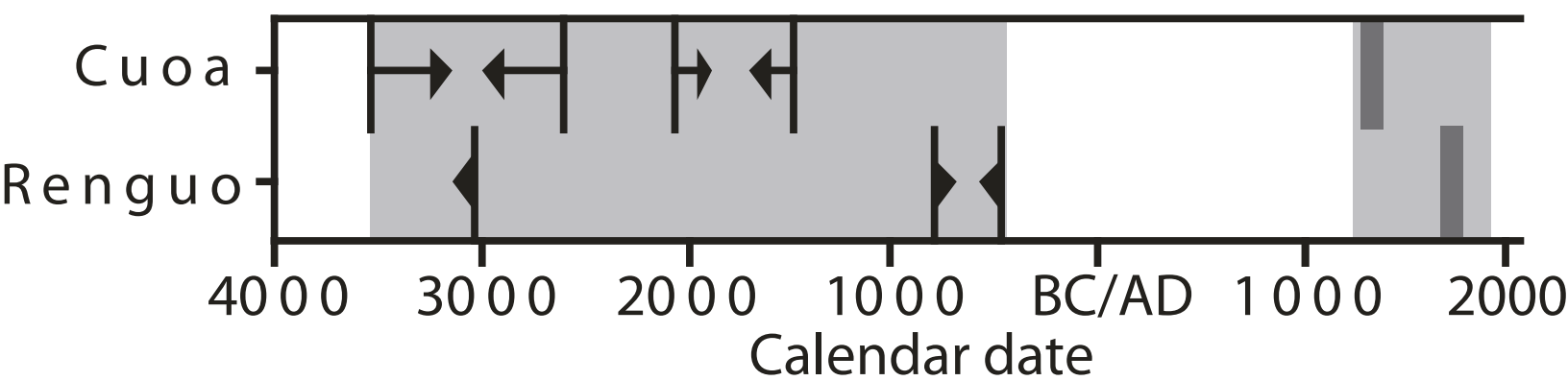



Figure13



-  Paleoearthquake events from Renguotrench
-  Paleoearthquake events from Cuatrench
-  Active period
-  Historical earthquake